The Thesis Committee for Garrett Lance Anderson
Certifies that this is the approved version of the following thesis:

Simulation of a Parallel Hydraulic Hybrid Refuse Truck

APPROVED BY
SUPERVISING COMMITTEE:

Supervisor: _____
Ronald D. Matthews

Co-Supervisor: _____
Raul G. Longoria

Simulation of a Parallel Hydraulic Hybrid Refuse Truck

by

Garrett Lance Anderson, B.S.

Thesis

Presented to the Faculty of the Graduate School of

The University of Texas at Austin

in Partial Fulfillment

of the Requirements

for the Degree of

Master of Science in Engineering

The University of Texas at Austin

December 2011

Dedication

I would like to dedicate my thesis to my both my immediate and extended family. I would not have been able to complete my graduate education without the support, patience, and assistance that they have provided.

Acknowledgements

I would like to thank Dr. Ron Matthews and Rob Harrison for the opportunities that they have provided me through research and funding opportunities. I also appreciate the patience that they have shown while working with me when things have taken longer than expected or not worked as planned.

Abstract

Simulation of a Parallel Hydraulic Hybrid Refuse Truck

Garrett Lance Anderson, M.S.E.

The University of Texas at Austin, 2011

Supervisor: Ronald D. Matthews

Co-Supervisor: Raul G. Longoria

A rear loading refuse truck was simulated with a conventional and hydraulic hybrid configuration. Models for the hydraulic hybrid components were developed to simulate the system. A control algorithm was developed using a stochastic dynamic programming approach. The results did not match those that are advertised by the commercially available systems, but reasons for this deviation are discussed. The predicted improvement in fuel economy ranged from 1% to 15% depending on variance in drive cycle and vehicle weight. A brief analysis of the cost of the hybrid system was also conducted based on an estimated drive cycle. This analysis showed that, at current fuel prices of about $4.00/gallon, the system may not make financial sense for a 10 year period of ownership.

Table of Contents

List of Tables ix

List of Figures xi

Chapter 1: Introduction 1

1.1. Hydraulic Hybrids: Benefits & Overview 2

1.2. Thesis Objectives & Overview 5

Chapter 2: Literature Review 6

2.1 Vehicle Modeling & Testing 6

2.2 Component Modeling 8

2.2.1. Pump Efficiency Models 8

2.2.2. Hydraulic Accumulator Model 10

2.2.3. Control Strategies 12

Chapter 3: Vehicle Specifications and Duty Cycle 14

3.1 Vehicle Specifications 14

3.1.1 Base Truck Specifications 14

3.1.2 Hybrid System Parameters 18

3.1.3 Refuse Body Hydraulic Circuit 20

3.2 Duty Cycle 21

Chapter 4: Component Models 23

4.1 Vehicle Model 23

4.2 Pump /Motor Model 24

4.2.1 Pump Efficiencies 25

4.2.2 Motor Efficiencies 25

4.3 Accumulator Model 29

4.4 Transfer Case 37

4.5 Hose Losses 38

4.6 Refuse Body Hydraulic Circuit 41

4.7 Control Strategy 44

Chapter 5: Vehicle Simulation and Results 54
5.1 Simulation method 54
5.2 Vehicle Simulation Sensitivity 57
5.2.1 Pump Efficiency Sensitivity 57
5.2.2 Accessory Loads 61
5.2.3 Transmission 63
5.2.4 Accumulator Time Constant 66
5.3 Vehicle performance 68
5.3.1 Vehicle Weight & Hydraulic System Load 68
5.3.2 Final Estimated Fuel Economy 72
Chapter 6: Hybrid System Cost Analysis 75
6.1 Estimated Hybrid System Maintenance Costs 75
6.2 Economic Analysis 80
Chapter 7: Conclusions and Future Work 84
7.1 Future Work 85
Appendix A: Drive Cycles 87
Bibliography 91

List of Tables

Table 1. Average power requirements of various accessory loads for local haul applications (SAE Truck and Bus Engine Preformance and Application Subcommittee, 2000). 17

Table 2. Selected parameters for a conventional refuse truck. 18

Table 3. Known system parameters for the Eaton HLA hydraulic hybrid system.19

Table 4. Parameters found in the literature used to match data for a high efficiency bent axis pump (Shan, 2009). 26

Table 5. Estimated constants used to predict the efficiency of the A4VSO piston pump. 28

Table 6. Constants used with the Benedict-Webb-Rubin equation to predict real gas behavior of nitrogen (Cengel, 2001). 31

Table 7. Dimensions of the bladder accumulator used in the present vehicle simulation (Eaton Corporation, 2005). 34

Table 8. Parameters used for estimating pressure drop in hoses and tubes (Esposito, 2003; Manring, 2005). 40

Table 9. Diameter and estimated lengths of hoses used in the modeled hybrid system (Eaton Corporation, 2011d). 41

Table 10. Simulation results that evaluate impact of pump efficiency maps with only accessory loads.....58

Table 11. Simulation results that evaluate the impact of pump efficiency that neglect accessory loads and includes the refuse body hydraulic system load.59

Table 12. The predicted fuel economy of hybrid vehicle with and without air conditioning. 62

Table 13. Gear ratios for alternate transmission used to evaluate effect of transmission used in model. 64

Table 14. Percent increase in fuel economy for implementation of hybrid system with 10 speed transmission over two conventional transmission configurations. 64

Table 15. Fuel economy of hybrid truck with varying time constant for the accumulator. 67

Table 16. Estimated fuel economy for various vehicle configurations for hypothetical drive cycle. 74

Table 17. Hydraulic hybrid maintenance items and estimated costs for each item including labor. 80

List of Figures

Figure 1. Basic representation of a typical hydraulic parallel hybrid 4

Figure 2. Basic representation of a typical hydraulic series hybrid. 5

Figure 4. Basic variable displacement bent axis piston pump design (Eaton Corporation, 2006). 9

Figure 5. Basic variable displacement axial piston pump design (Eaton Corporation, 2006). 9

Figure 6. Cross section of bladder type hydraulic accumulator (Eaton Corporation, 2006). 11

Figure 7. Cross section of piston type hydraulic accumulator (Eaton Corporation, 2006). 12

Figure 8. Image of a Peterbilt 320 refuse truck (Peterbilt Motors Company, 2010). 14

Figure 9. Line drawing of the Eaton Hydraulic Launch Assist hydraulic hybrid system (Eaton Corporation, 2011d). 19

Figure 10. Refuse body pump flow and power requirement as a function of speed (Geartek, 2008). 20

Figure 11. Estimated efficiency map of the bent axis pump presented in a 2004 EPA report. 27

Figure 12. Estimated efficiency maps for the A4VSO piston pump. 28

Figure 13. Pressure as a function of oil volume for a 15 gallon accumulator with various assumptions about gas behavior. 30

Figure 14. Cross section of a bladder type accumulator and labeled dimensions corresponding to values in Table 7 (Eaton Corporation, 2005). 34

Figure 15. Pressure vs. time of an accumulator being filled with 7 gallons or fluid at varying rates. 35
Figure 16. Pressure vs. oil volume of an accumulator being filled with 7 gallons or fluid at varying rates. 36
Figure 17. Temperature vs. time of an accumulator being filled with 7 gallons or fluid at varying rates. 36
Figure 18. Representation of transfer case used to connect the pump to the drivetrain. 37
Figure 19. Predicted efficiency of the transfer case used with the modeled hybrid system. 38
Figure 20. Estimated pressure drop per foot for several diameters of hose. 40
Figure 21. Estimated gear pump efficiency based on data from the pump specification sheet (Geartek, 2008). 42
Figure 22. Schematic of the hydraulic circuit for the refuse body. 42
Figure 23. Open center pressure drop of various components in the refuse body hydraulic circuit. 43
Figure 24. Estimated torque and power requirement of the hydraulic system pump. 44
Figure 25. Simulink diagram of the model used to estimate driver power demand over various drive cycles. 45
Figure 26. Fast Fourier transform of several drive cycles for verification of the filter cutoff frequency. 46
Figure 27. Visual representation of the transition probability matrix used to develop a Markov Chain of driver power demand and vehicle speed. 47
Figure 28. Power split ratio map for a wheel speed of 6 rad/s. 53

Figure 29. Effect of initial accumulator charge on fuel economy for various drive cycles.....55
Figure 30. Percent difference in fuel economy based on initial state of accumulator as a function of drive cycle repetitions.....56
Figure 31. A Comparison of the accumulator volume for the two evaluated pump efficiency maps during the first 55 seconds of ten CBD drive cycle.59
Figure 32. A Comparison of the pump displacement for the two evaluated pump efficiency maps during the first 55 seconds of the CBD drive cycle.60
Figure 33. A Comparison of the pump efficiency for the two evaluated pump efficiency maps during the first 55 seconds of the CBD drive cycle.61
Figure 34. Speed profile of New York Garbage Truck drive cycle.....63
Figure 35. Estimated torque ratio and efficiency of two Allison torque converters available on 4000HS series transmission.....66
Figure 36. Estimated fuel economy and percent improvement of refuse truck as weight varies for CBD drive cycle.....69
Figure 37. Speed vs. time profile of Central Business District Cycle. 70
Figure 38. Estimated fuel economy and percent improvement of refuse truck as weight varies for HUDDS drive cycle. 71
Figure 39. Speed vs. time profile of Heavy Duty Urban Dynamometer Driving Schedule. 71
Figure 40. Speed profile of hypothetical drive cycle that was generated from a combination of the HUDDS and CBD cycles.....72
Figure 41. Addition of weight as a function of time for hypothetical drive cycle.73
Figure 42. Reasons for adopting green fleet practice for beverage distributors (Cioletti et al., 2011). 75

Figure 43. Line drawing of Eaton Hydraulic Launch Assist sytem (Eaton Corporation, 2011d). 76
Figure 44. Exploded view of main system oil filter (Eaton Corporation, 2011d).78
Figure 45. Cross sectional view of bladder type accumulator (Eaton Corporation, 2006). 79
Figure 46. Replacement accumulator bladder cost per gallon as a function of bladder size (McMaster-Carr, 2011). 79
Figure 47. Estimated cost of hybrid system ownership for a hydraulic hybrid refuse truck without hydraulic system load. 82
Figure 48. Estimated cost of ownership for a hybrid system that includes load from the hydraulic system. 83
Figure 49. Speed profile of Central Business District drive cycle. 87
Figure 50. Speed profile of Heavy Duty Urban Dynamometer Driving Schedule.87
Figure 51. Speed profile of Manhattan drive cycle. 88
Figure 52. Speed profile of New York Garbage Truck drive cycle. 88
Figure 53. Speed profile of New York Truck drive cycle. 89
Figure 54. Speed profile of Orange County Bus drive cycle. 89
Figure 55. Speed profile of West Virginia University City drive cycle. 90

Chapter 1: Introduction

The world population is increasing and is estimated to reach 9 billion by the year 2050. Of those 9 billion people, 6 billion are expected to live in cities. The world population grew from 250 million to 2.8 billion in the 20th century (Ratti et al., 2011). During that period many issues had to be overcome to provide residents with a healthy environment in which to live.

The U.S. population is expected to grow by 85.6 to 106.9 million people by the year 2040 from the current population of 308.7 million, and the Texas population is predicted to grow by 14.9 million people from the current population of 25.1 million (U.S. Census Bureau, 2009; Texas State Data Center, 2009). This addition to the population will create a larger demand for freight to bring in the goods that people require and also to dispose of their refuse. This addition in population should also create an increase in jobs which will most likely cause an increase in raw materials, equipment, produced goods, and services which will all have some requirement for transportation.

A large percentage of the additional growth in Texas is predicted to occur in what is known as the "Texas Triangle" megaregion. A megaregion is made up of two or more metropolitan areas that are linked through multimodal transportation infrastructures, environmental systems, and complimentary economies. Megaregions have the benefit of concentrating people, jobs, and capital which makes them attractive in a global economy (Butler, Hammerschmidt, Steiner, & Zhang, 2009).

This increase in population and freight in a confined region will cause an increase in vehicle emissions which can consist of particulate matter, carbon monoxide, carbon dioxide, oxides of nitrogen, and hydrocarbons. All of these compounds can have an effect on people and the environment. The problems that they create can include

respiratory issues, corrosion of a wide variety of materials, acid rain, and even death in certain individuals (U.S. Environmental Protection Agency Office of Air and Radiation, 2011).

It is quite clear that the growing freight demand in Texas will require a more efficient transportation system at many levels. Many solutions will be required to accomplish this, and hybrid trucks offer a potential to fill a niche in urban environments where a large amount of starting and stopping are required. Their adoption could potentially reduce emissions and fuel consumption.

1.1. HYDRAULIC HYBRIDS: BENEFITS & OVERVIEW

A hybrid drivetrain is a system consisting of two or more types of power sources that are used to propel a vehicle. A typical hybrid drivetrain consists of an internal combustion engine, the required drivetrain components to transmit the power to the ground, and an alternative energy source that can both provide power and store energy for later use. There are many different combinations of vehicle architectures, alternative energy sources, and control strategies that can be implemented in a hybrid vehicle. Some of these components, strategies, and systems are better suited for certain applications than others (Ehsani, Gao, & Emadi, 2009).

The hydraulic hybrid system, which is the focus of this thesis, uses hydraulic pump/motors, valves, and accumulators to store and release energy during the drive cycle. There are several benefits to this system. The first is that it has a very high power density which allows the system to assist a great deal with launch and braking events. The Hydraulic Launch Assist (HLA) system that Eaton sells has an estimated maximum power of 380 hp. The second benefit is that it has the potential to use many off the shelf components which greatly reduces the cost. Estimated costs for the system range from

$7,000 to $38,000 (Eaton Corporation, 2009; Gray Jr, 2006). If the cost of the base truck is assumed to be $200,000, the percent increase in the cost of the truck is anywhere from 4% to 19%. The third benefit of the system is that brake wear can be significantly reduced because the hybrid system is recovering that energy rather than the brakes dissipating it as heat. The city of Denver estimates that it services the brakes every 3 to 4 months on its conventional refuse trucks at a cost of $2,000 per incident. Eaton advertises that their HLA system can double brake life (Eaton Corporation, 2009). Studies conducted on another system manufactured by Parker Hannifin found that the system increased the brake change interval to 102 weeks from 12 weeks for a refuse truck (Soderberg, 2011)

However, there are some disadvantages for this system. The first is that it does not have the capacity to store large amounts of energy, in contrast to batteries. This can limit the duration of time for which the system can assist with braking and acceleration. The second disadvantage is that the system does add a considerable amount of weight to the vehicle which reduces the amount of weight available for cargo. Eaton advertises a system weight of 1,350 lbs (Eaton Corporation, 2009). The assumed gross vehicle weight rating for the refuse truck in this study is 56,000 lb. The tare weight is assumed to be 33,000 with the hybrid system. Therefore, the conventional truck could legally carry almost 5.8% more weight.

The hydraulic hybrid is available in several different architectures. The two configurations that have seen the most interest are the parallel and the series hybrid configurations.

The hydraulic parallel configuration typically differs from that of the electric hybrids that are commercially available in how the two powertrains are joined together. The typical heavy duty electric hybrid places the motor/generator between the engine and

transmission while the hydraulic hybrid ties the two powertrains together through a transfer case between the transmission and differential. The transfer case also contains a clutch that enables the pump/motor to be disengaged at higher speeds. This configuration is illustrated in Figure 1.

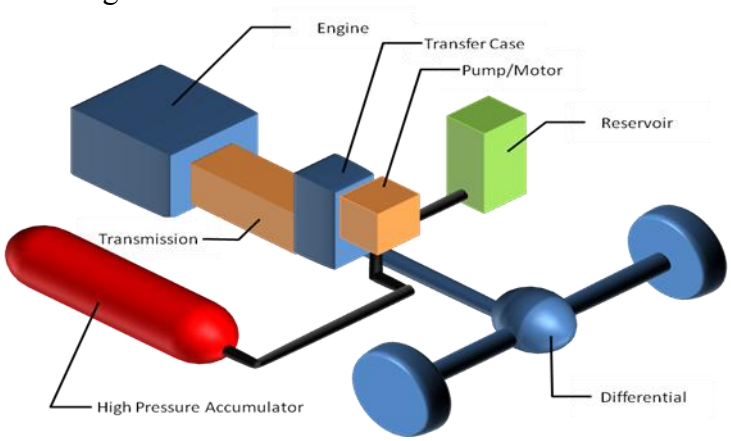

Figure 1. Basic representation of a typical hydraulic parallel hybrid

The hydraulic hybrid series configuration is much like the electric hybrid series configuration. There is a pump mounted directly to the engine which is connected to a high pressure accumulator and hydraulic motor. In this configuration there is no direct mechanical path from the engine to the rear wheels. This configuration is illustrated in Figure 2.

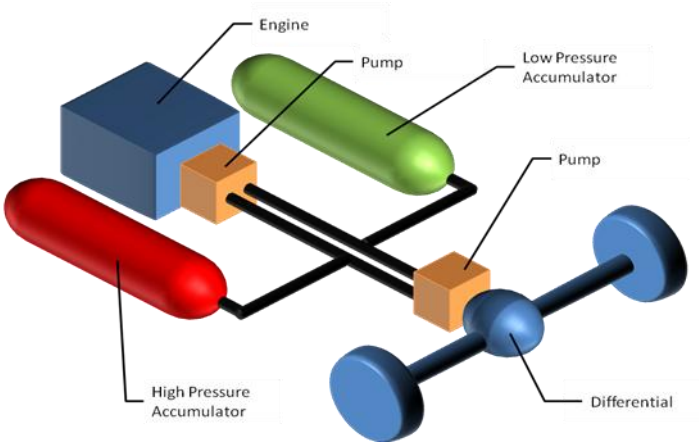

Figure 2. Basic representation of a typical hydraulic series hybrid.

1.2. THESIS OBJECTIVES & OVERVIEW

The focus of this thesis research was to model a parallel hybrid refuse truck to predict its fuel economy. This data was then used to estimate the difference in operating costs and the amount of time that the system will take to have a return on investment.

Currently there is not a great deal of information pertaining to the economics of heavy duty hybrids. Despite the fact that these systems do reduce fuel consumption and brake wear, they have an initial increase in cost of the vehicle and additional maintenance requirements.

The following chapter contains a literature review of hydraulic hybrid vehicles that have been modeled with a brief description of what assumptions were made. This is followed by a chapter with the vehicle specification for the study and a description of its assumed duty cycle. Chapter 4 explains the component models that were used and justifications for their use. The results of the simulation are then presented in Chapter 5, and then the conclusions reached by the study are presented in Chapter 6.

Chapter 2: Literature Review

While interest in hydraulic hybrids may have only increased recently, the first paper published on the subject by Dunn and Wojciechowski (1972). Since that time many different hydraulic hybrid vehicles have been modeled and built by various universities and organizations.

2.1 Vehicle Modeling & Testing

In 2004 the EPA issued a report on several advanced automotive technologies that they had developed. One of these technologies was hydraulic hybrids. In this report the EPA modeled a large, 4-wheel drive SUV and a mid-size, front wheel drive sedan with several different powertrain and control strategy configurations. The estimated increase in fuel economy with a conventional gasoline engine ranged from 17% to 34% for the large SUV and 12% to 50% for the sedan. Other information presented in the report pertained to improvements made to individual components to increase the efficiency of the system. These included modifications of the accumulator and pump and will be discussed in subsequent sections (Advanced Technology Division, 2004).

Figure 3. Hydraulic hybrid step van constructed through a partnership between UPS, Navistar, Eaton Corporation, and the EPA (Barry, 2008).

In addition to their modeling of hydraulic hybrids, the EPA has also converted several vehicles to hydraulic hybrids including a delivery step van, yard hostler truck, Ford Expedition, Ford F-550 pickup, and a large sedan test chassis. The delivery step van was constructed as a series hybrid in conjunction with UPS, Navistar, Eaton Corporation, Parker-Hannifin, the U.S. Army, FEV, Morgan-Olson, and Southwest Research Institute and is shown in Figure 3. A total of seven of these vehicles were constructed and tested in the Minneapolis area, and they achieved a 60-70% increase in fuel economy (United States Environmental Protection Agency, 2010).

The University of Michigan has been very active in hybrid research in general and has also modeled several hydraulic hybrids. These vehicles include a Humvee, a medium duty delivery truck, and a 6X6 medium duty truck. The two medium duty trucks were modeled as parallel hybrids while the Humvee was modeled as a series hybrid. The study of the 6X6 truck estimated a 32% improvement in fuel economy. They also estimated that 2/3 of the improvement was attributed to the optimal sizing of components (Filipi et al., 2004). The estimated increase in fuel economy for the delivery truck ranged from 15.6% to 76.8% depending on the vehicle control strategy and assumed drive cycle (Bin Wu, Lin, Filipi, Peng, & Assanis, 2004). The estimated increase in fuel economy for the Humvee was 68% for city driving with an engine off strategy. The improvement for highway driving was estimated to be 11-12% (Kim & Filipi, 2007).

A medium duty truck was also modeled at the University of Toledo with an emphasis on developing an advanced control strategy. The results of this study were validated with VPSET which is a software package developed by Southwest Research Institute. The resulting increase in fuel economy for the vehicle ranged from 44% to 135% depending on drive cycle and control strategy (Shan, 2009).

Another important study was conducted by Pourmovahed, Beachley, and Fronczak. Their study analytically evaluated the regeneration of energy from a flywheel. This work was published in 1992 and has been cited by the studies conducted at Toledo and Michigan for the modeling of many of the hydraulic components.

2.2 COMPONENT MODELING

In order to model a hydraulic hybrid, models for several hydraulic components must be constructed in addition to the base vehicle model. These components include the pump/motor, hydraulic accumulator, and various control strategies. The discussion in this section will include a brief description of what models have been used for each of these components. An in depth discussion of the models used for the present study can be found in Chapter 4.

2.2.1. Pump Efficiency Models

An accurate estimate of the pump efficiency is critical for the prediction of the fuel economy of the vehicle because it is responsible for converting energy between the mechanical drivetrain and the hydraulic system. There are several common types of hydraulic pumps and motors. These include gear, vane, and piston pumps. However, piston pumps are the primary type of pump used in hydraulic hybrids because of their high efficiency, high pressure capability, and because they are commonly available with a variable displacement.

The torque of a pump or a motor is a function of pressure and displacement. While it is possible to vary the pressure seen by the pump by restricting the flow with a valve, it is not the most efficient way to vary the pump torque. These flow restrictions also cause a corresponding power loss to their pressure reduction. This makes variable displacement a very important feature for a pump to have in this particular application

because it allows for the input torque of the pump to be varied without creating a large power loss.

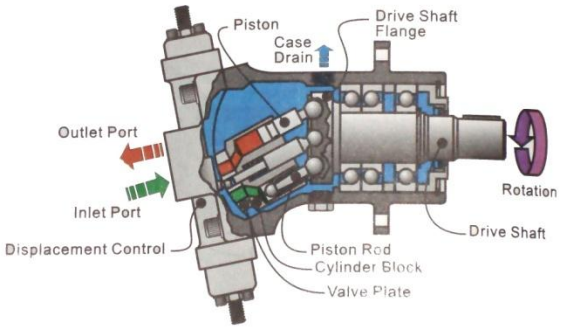

Figure 4. Basic variable displacement bent axis piston pump design (Eaton Corporation, 2006).

There are two types of piston pumps that are commonly used in hydraulic hybrids. These two types are a "bent axis" piston pump shown in Figure 4 and an "axial" piston pump shown in Figure 5. The axial piston pump is used in systems available from Eaton and Bosch Rexroth, while the bent axis type pump has been extensively used in research conducted by the EPA.

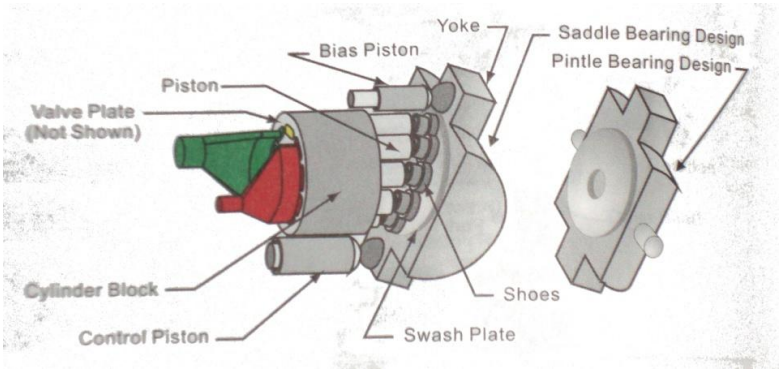

Figure 5. Basic variable displacement axial piston pump design (Eaton Corporation, 2006).

Two strategies were found in the literature for modeling of piston pumps. The first method was developed by (Abuhaiba & Olson, 2010) and used a geometric model to predict noise and vibrations generated by the pump. This approach models the individual interfaces within the pump. The second method is based upon "Wilson's Pump Theory". This method was employed by all the studies mentioned previously with the exception of the EPA (Filipi et al., 2004; Kim & Filipi, 2007; Pourmovahed, Beachley, & Fronczak, 1992; Shan, 2009; Bin Wu et al., 2004). The goal of this method is to recognize that certain kinds of losses will occur within the pump to build a semi-empirical model that estimates the volumetric and mechanical efficiencies. Methods presented in Hydraulic Control Systems (Merritt, 1967), Hydraulic Control Systems (Manring, 2005), and Hydraulic Power System Analysis for fixed displacement pumps all closely resemble this method (Akers, Gassman, & Smith, 2006). More detail on this method can be found in Chapter 4.

2.2.2. Hydraulic Accumulator Model

The hydraulic accumulator is the portion of the hybrid system that is responsible for storing energy as compressed gas. They are available in many configurations that include spring, piston, diaphragm, and bladder type accumulators. The specific type used by the Eaton HLA system is a bladder type accumulator which is depicted in Figure 6. This type of accumulator utilizes a rubber bladder filled with compressed nitrogen to store energy.

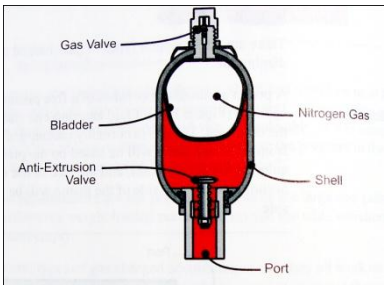

Figure 6. Cross section of bladder type hydraulic accumulator (Eaton Corporation, 2006).

Because the accumulator is filled with nitrogen, it is common to assume that it behaves like an ideal gas. However, since the nitrogen is exposed to high pressures, the ideal gas assumption has the potential to break down. Two different approaches were found when making this assumption. Karnopp, Margolis, and Rosenberg (2006) recommend modeling it as an isentropic process while Akers, Gassman, and Smith (2006) recommend treating the process as polytropic. These approaches both have the benefit of being simple by yielding an algebraic equation to model the process.

Another approach was found that treated the nitrogen as a "real" gas by using the Benedict-Webb-Rubin equation of state (Otis & Pourmovahed, 1985). This method also accounted for the heat transfer from the nitrogen to the wall of the accumulator. This particular study analyzed a piston type accumulator which can be seen in Figure 7. Despite the fact that they analyzed a different type of accumulator, there are still many fundamental concepts that are used later to model the bladder type accumulator.

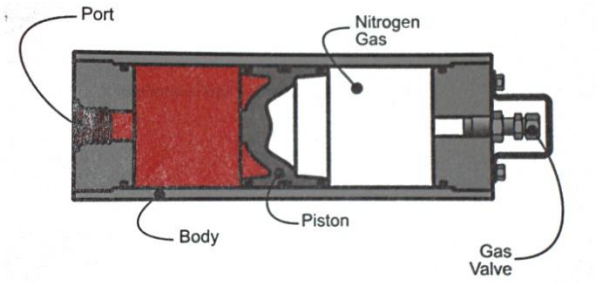

Figure 7. Cross section of piston type hydraulic accumulator (Eaton Corporation, 2006).

2.2.3. Control Strategies

The control strategy is a very important aspect of a hybrid vehicle. Regardless of the architecture, there exist two main classifications of control strategies. These strategies are rule based and optimization based strategies. Within each of these two categories there are additional classifications that contain strategies that have their own strengths and weaknesses (Desai & Williamson, 2009).

Rule based strategies are based on rules specified by the engineer designing the system. These rules typically seek to optimize a single parameter like fuel consumption. These strategies are usually very simple and easy to implement, but they typically only look to optimize a single parameter (Desai & Williamson, 2009).

Optimization based strategies seek to find the most efficient operating strategy for a vehicle through a given drive cycle or set of drive cycles. These strategies can take into account the efficiencies of several components in the system much more easily. They are also able to easily optimize vehicle operation based on several parameters. These parameters could include but are not limited to fuel consumption and various engine emissions (Desai & Williamson, 2009).

Two optimization based techniques that were found in the literature were based upon deterministic dynamic programming and stochastic dynamic programming.

The process followed by the deterministic approach involved using only the positive power demand of the driver for the dynamic programming algorithm to find the optimal "power split ratio" (PSR) and gear shift strategy as a function of time for a given drive cycle. The use of only the positive power demand was done to make the strategy charge sustaining. The operating points of the optimal trajectory were then plotted as PSR vs. power demand to allow for the fitting of a curve to the data. The gear shift strategy was determined by plotting the operating points for each gear with vehicle speed along the x axis and power demand on the y axis. The operating points were then fit into regions to develop a shift strategy (Chan-Chiao Lin, Huei Peng, Grizzle, & Jun-Mo Kang, 2003).

The stochastic approach seeks to use information about past or potential drive cycles to predict the future operating points of the vehicle. To solve the problem in this form, the driver power demand was modeled as a Markov Chain. The vehicle speed and state of charge of the battery were then assumed to be deterministic processes to formulate a Markov Decision Process. The optimal control policy was then solved for using policy iteration. The result of this process is a control policy that is directly implementable and does not require a curve fitting procedure. Both approaches were compared in the present research, and the stochastic process was found to perform slightly better over a wide range of cycles (Chan-Chiao Lin, Huei Peng, & Grizzle, 2004).

Chapter 3: Vehicle Specifications and Duty Cycle

Determining the specifications for a typical refuse truck is somewhat of a difficult task. This is caused by the fact that there are many truck manufacturers and many companies that construct refuse truck bodies. Each one of these companies may offer several models that are each well suited for a specific application. This leads to a very large variety of refuse trucks that make up the entire population.

3.1 Vehicle Specifications

The truck selected as the representative model was a Peterbilt 320 with a 25 yd^3 rear loading refuse truck body. The hybrid system selected was the Eaton Hydraulic Launch Assist system. This configuration was selected based on vehicle usage, commercial availability, and the availability of data.

Figure 8. Image of a Peterbilt 320 refuse truck (Peterbilt Motors Company, 2010).

3.1.1 Base Truck Specifications

The primary reason that the Peterbilt 320 model was chosen as the base vehicle is because it is commercially available with a hydraulic hybrid system. A brief survey of the internet found that there is a wide selection of used 320's available. Similar models

are available from Mack Truck and Crane Carrier Company that are also very popular for use as refuse trucks. When selecting parameters for the vehicle, the Peterbilt 320 was used as the primary source of information when possible.

Two of the most important parameters of the vehicle are the gross vehicle weight rating (GVWR) and its tare weight. The difference between these two values will determine its capacity for cargo or refuse.

The GVWR was determined to be 56,000 lb. This was based on the required GVWR for a Leach brand 25 yd^3 refuse body (Labrie, 2010). While the 320 is available with a single front axle rated at 20,000 lb and tandem rear axles rated for 46,000 lb, the State of Texas does not allow a triple axle vehicle to legally operate over 60,000 lb without special permits (Peterbilt Motors Company, 2011; Texas Dept. of Transportation, 2011). Therefore, it was assumed that the truck would be configured to meet the requirement of the refuse body.

The tare weight of the vehicle was estimated to be 33,000 lb. This weight was based on an estimate published in a hydraulic hybrid feasibility study conducted by vePower Technologies ((Canada), Drozdz, & Technologies, 2005). The additional weight of the assumed refuse body was 15,800 lb. This is the weight of the Leach 25 yd^3 refuse body (Labrie, 2010). Based on these estimates, the base truck would weigh 17,200 lb which seemed reasonable. The tare weight of commercial trucks is not commonly available because of the large amount of possible configurations.

The frontal area of the vehicle is also required in order to estimate aerodynamic losses of the vehicle. This value was estimated to be 75 ft^2. While this area does seem very large, it does include the area of the refuse body as well. The assumed refuse body has a height of 93” and a width of 96”. The height is specified as the height above the top of the frame rail of the truck. Because of the height of the tires, which are discussed

later, the frame rails must be around 4' above the ground. This yields a total height of 11.75'. The resulting area is 94 ft^2. Wong states in the "Theory of Ground Vehicles" that the frontal area for passenger cars varies between 79% and 84% of the area calculated from the overall height and width of the vehicle (Wong, 2008). Even though this value is for passenger vehicles, a value of 80% was used to estimate the actual area of the refuse truck. More investigation was not conducted because a refuse truck does not operate at high speeds for significant portions of time where aerodynamic losses are greatest. Therefore a more accurate estimate for this value would most likely not yield a significant increase in accuracy of the model.

The engine was assumed to be rated for 325 hp (242 kW). This was based on several factors. The first piece of data was a study conducted for the City of New York. The study states that the trucks involved with the study used an engine rated at this power (Ivanič, 2007). A quick survey of new Peterbilt 320's showed that the truck was available with a 320 hp engine and that it was a commonly available in this configuration (Rush Enterprises, 2006).

In addition to the required torque to drive the vehicle are the accessory loads. These loads can include but are not limited to power steering pumps, A/C compressors, air brake compressors, and cooling fans. The estimated power requirements for these loads were taken from SAE Specification J1343. This specification contains estimates for the power requirements of these types of loads for various applications. The values used for the present model can be found in Table 1. While most of these loads will be intermittent, they were considered to be on continually with the torque varying with engine speed to maintain a constant power.

Table 1. Average power requirements of various accessory loads for local haul applications (SAE Truck and Bus Engine Preformance and Application Subcommittee, 2000).

System	Average Load (hp)
Air Brake Compressor	4.6
A/C Compressor	3
Engine Fan	4
Power Steering Pump	9

The selection of the transmission was a major deviation between the model and the actual vehicle. The 320 is available with an Allison automatic transmission that has 4, 5, or 6 forward speeds or a manual Eaton transmission (Peterbilt Motors Company, 2011). Because of the lack of availability of a torque converter type automatic transmission model or data, the model assumed that the transmission would be an automated manual. Data for gear ratios were taken from the specification sheet for an Eaton UltraShift Plus VAS. This specific model is a 10-speed automated manual which is approved for refuse applications (Eaton Corporation, 2011a).

The truck was assumed to be configured with tandem drive axles in order to meet the weight requirements of the truck. The final ratio of the differential was selected from the set of gear ratios available for the Dana Spicer D170 series tandem axle (Eaton Corporation, 2011b). The ratio that yielded the best performance was 5.38. Other requirements like gradeability may dictate this ratio in certain applications but were not considered for the present study.

The 320 is available with 22.5” rims (Rush Enterprises, 2006). The tires recommended by Michelin Tire for refuse trucks in the drive position and this wheel size range from 42.2” to 43.3” in diameter. The loaded radius of the recommended tires varied from 19.8” to 20.0” (Michelin, 2011).

Table 2. Selected parameters for a conventional refuse truck.

Parameter	Value
Tare Weight (lb)	33,000
GVWR (lb)	56,000
Height (in)	141”
Width (in)	96”
Tire Diameter	40”
Differential Ratio	5.38
Transmission Ratios (Eaton Corporation, 2011c)	12.8, 9.25, 6.76, 4.90, 3.58, 2.61, 1.89, 1.38, 1.00, 0.73

3.1.2 Hybrid System Parameters

Many parameters for the hybrid system were required for the modeling of the hybrid system. Some of the parameters were found in the service manual and other promotional material. However, some parameters were estimated based on other information. A line drawing of the system can be seen in Figure 9, and the system parameters that were known can be found in Table 3.

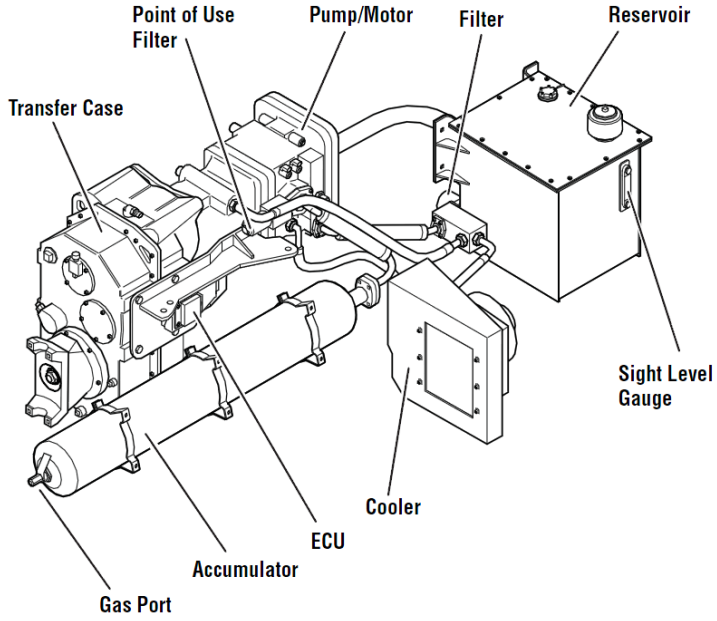

Figure 9. Line drawing of the Eaton Hydraulic Launch Assist hydraulic hybrid system (Eaton Corporation, 2011d).

Table 3. Known system parameters for the Eaton HLA hydraulic hybrid system.

Parameter	Value
Maximum system pressure	5000 psi
Maximum pump speed	3000 rpm
Estimated maximum power	380 hp
Pump Displacement	15.26 in^3/rev
Fluid Capacity	21 gallons
Total Weight	1350 lbs

The exact size of the accumulator was not known. Because the fluid capacity of the system is known to be 21 gallons, an upper limit can be placed upon the accumulator volume. This limit is well below the full system capacity because there must always be fluid left in the reservoir to protect the pump, fluid contained with the pump case, and fluid within the various hoses. The accumulator was also known to be a bladder type

accumulator that weighs 380 lb (Eaton Corporation, 2011d). After consulting the Eaton accumulator catalog, a 15 gallon bladder type accumulator was found that weighed 370 lb and was rated for 5000 psi (Eaton Corporation, 2005).

3.1.3 Refuse Body Hydraulic Circuit

The final aspect of the vehicle that must be modeled is the hydraulic circuit for the refuse body. To estimate parameters for this portion of the system, specification sheets for various refuse bodies were consulted to understand the typical configuration. However, for exact specifications the specification sheet for the Leach 2R-III body was used.

The pump for this system is a gear pump that is rated for 42 gpm at 1200 rpm (Labrie, 2010). The pump selected for this application was a GearTek D45 gear pump. This particular pump is an 8.94 in^3/rev, cast-iron gear pump rated for 2500 psi (Geartek, 2008). The advertised flow as a function of speed is shown in Figure 10.

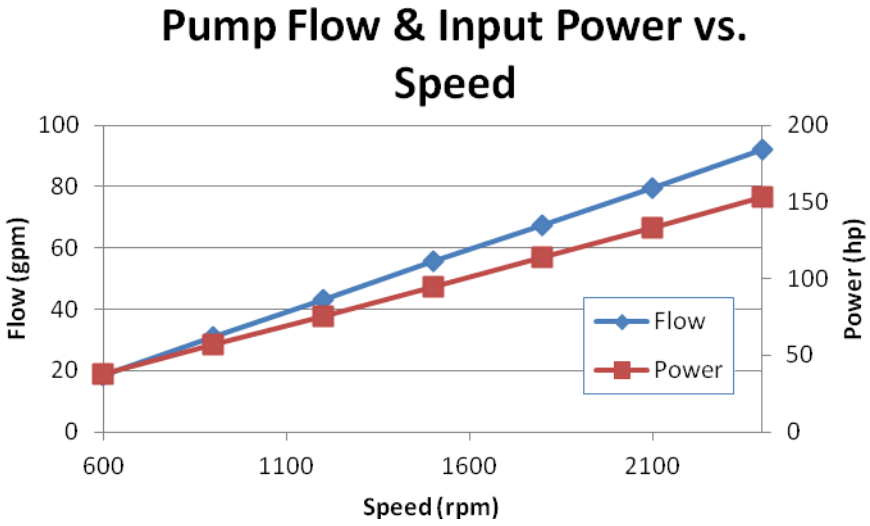

Figure 10. Refuse body pump flow and power requirement as a function of speed (Geartek, 2008).

Because a gear pump is a fixed displacement pump, the system was assumed to be an open center system. Open center means that when the system is not being actuated, there is a flow path directly through the control valve back to the reservoir (Eaton Corporation, 2006). The control valve selected for the model was a Munsie 90V Sereis valve which is an open center valve which is rated for 90 gpm and approved for refuse truck applications. A valve this large was chosen to reduce the losses when the engine is operating at speeds in excess of 1200 rpm.

This pump is commonly mounted directly to the engine or on a PTO that can be disengaged. Since both of these options seem to be common, the system was modeled with and without this load for most situations.

3.2 DUTY CYCLE

Refuse trucks operate under very extreme conditions with very frequent starting and stopping. This leads to very poor fuel economy. These trucks have actual fuel economies that range from 1.3 to about 2.8 mpg (Chandler, Norton, & Clark, 2001; Ivanič, 2007). The average refuse truck for the city of Denver travels 8400 miles annually with an average fuel economy of 2.3 mpg (Eaton Corporation, 2009). Based on these figures, the average Denver truck consumes about 3650 gallons of fuel per year.

The Denver operating conditions are just one data point in a much larger picture. In 2007, a study was conducted on New York City garbage trucks to determine the average New York City refuse truck drive cycle. During the study 450 hours of data were collected on various routes to compile a final cycle. The results showed an average fuel economy of 1.3 mpg with an average speed of 4.1 mph. The paper also states that the trucks were operated 6 days a week. If a 10 hour work day was assumed, it could be estimated that the annual mileage of the truck would be 10,234 miles/year (Ivanič, 2007).

A study conducted by the NREL in Washington, PA estimated that the annual mileage of one group of the trucks in their study was much higher at 27,540 miles/year with an average speed of 11.5 mph. The other group of trucks in the study were LNG trucks that had similar statistics that were slightly less extreme because closer routes were specifically chosen for these trucks because of uncertainty about their reliability at that time. Under these conditions the Waste Management trucks averaged about 2.8 mpg (Chandler et al., 2001). Refuse truck annual utilization will have a wide range of values, since some metropolitan areas have several processing sites, while others may only have a single remote processing facility.

Further investigation into the large discrepancy of these datasets found that Washington, PA only has a population of about 15,000 (City of Washington, PA, 2011). It is suspected that the trucks operating in the NREL study had routes that were somewhat rural or suburban in nature.

As mentioned earlier, the City of New York has worked to define its typical refuse truck drive cycle. They found that the average speed of the truck is only 4.1 mph. This includes the trip to and from the landfill where the vehicle reaches speeds of up to 50 mph. However, the truck spends almost 75% of its time collecting garbage. During this operation the vehicle averages 1.1 mph with about 49 stops per mile (Ivanič, 2007).

Based upon this information appropriate drive cycles were selected to replicate the various modes of operation of a refuse truck. Drive cycles that were considered included but are not limited to the Orange County Bus Cycle, New York Garbage Truck Cycle, Heavy Duty Urban Dynamometer Driving Schedule, and the Central Business District Cycle. A full list of evaluated cycles can be found in Appendix A with the speed profile of the cycle.

Chapter 4: Component Models

Now that the vehicle is fully defined it is possible to create representative component models for the system. Efficiency maps for some of the components were already available. These components include the engine, transmission, and differential (R. D. Matthews et al., 2011). More detail about the assumptions made in generating these efficiency maps can be found in the referenced document.

4.1 Vehicle Model

The vehicle was modeled as a point mass to predict the road loads of the vehicle. These loads typically include aerodynamic drag, rolling resistance, and loads due to a grade. However, for this study the road was assumed to be flat which eliminates any loads caused by a grade. The resulting equation of motion for the vehicle is shown as Equation 1.

$$m_{eff}\, a = \tau_{wheel} R_{wheel} - F_{aero} - F_{roll} \tag{1}$$

$$m_{eff} = \frac{1.035 W_v + W_p}{g} \tag{2}$$

The mass used in Equation 1 above is known as the effective mass of the vehicle. This mass attempts to approximate the additional inertia of the rotating components of the drivetrain. The EPA developed the relation in Equation 2 and published it in 1978 (Ronald Douglas Matthews, 2010).

$$F_{drag} = \frac{1}{2} \rho_{air} C_d A_{front} V^2 \tag{3}$$

The aerodynamic resistance of the vehicle requires knowledge of the frontal area of the vehicle (A_f), drag coefficient (C_d), air density (ρ_{air}), and vehicle speed (V). Equation 3 was used to calculate this load. The density of air was assumed to be 0.002378 slugs/ft^3. The drag coefficient was assumed to be 0.8. This was based on the upper value of the range of drag coefficients presented for buses presented by (Wong, 2008). The frontal area was assumed to be 75 ft^2. A discussion of the estimation for this value can be found in Chapter 3.

$$F_{roll} = mgf_r \tag{4}$$

$$f_r = 0.006 + 0.23 \times 10^6 \times V^2 \tag{5}$$

The rolling resistance of the vehicle is calculated using Equations 4 and 5. It is very important to note that the vehicle speed V is specified in units of kph (Wong, 2008).

4.2 PUMP /MOTOR MODEL

The hydraulic pump/motor employed for this simulation was based upon "Wilson's Pump Theory". This model is a semi-empirical model that estimates both volumetric and mechanical efficiencies. The idea is that certain mechanical and volumetric losses will occur within the pump that create specific trends in the efficiency. Rather than attempt to model all of these losses, they are analyzed as a group to predict the efficiency map.

There are four equations for all of the efficiencies. This is caused by the fact that the volumetric and mechanical efficiency for a motor and a pump are the inverse of each

other. Equations 6 to 11 are the required set of equations to model the pump/motor over its entire operating range.

4.2.1 Pump Efficiencies

$$\eta_v = 1 - \frac{C_s}{|x|S} - \frac{\Delta P}{\beta} - \frac{C_{st}}{|x|\sigma} \tag{6}$$

$$\eta_m = \frac{1}{1 + \frac{C_v S}{|x|} - \frac{C_f}{|x|} + C_h x^2 \sigma^2} \tag{7}$$

4.2.2 Motor Efficiencies

$$\eta_v = \frac{1}{1 + \frac{C_s}{xS} + \frac{\Delta p}{\beta} + \frac{C_{st}}{x\sigma}} \tag{8}$$

$$\eta_m = 1 - \frac{C_v S}{x} - \frac{C_f}{x} - C_h x^2 \sigma^2 \tag{9}$$

$$S = \frac{\mu \omega}{\Delta p} \tag{10}$$

$$\sigma = \frac{\omega \sqrt[3]{D}}{\sqrt{\frac{2\Delta p}{\rho}}} \tag{11}$$

Table 4. Parameters found in the literature used to match data for a high efficiency bent axis pump (Shan, 2009).

Variable	Parameter	Value
β	Bulk Modulus (MPa)	1660
μ	Dynamic Viscocity (N-s/m^2)	0.034
ρ	Fluid Density (kg/m^3)	850
C_s	Laminar Leakage Coefficient	2.63E-09
C_{st}	Turbulent Leakage Coefficient	1.33E-07
C_v	Viscous Loss Coefficient	1.20E-04
C_f	Friction Loss Coefficient	1.01E-02
C_h	Hydrodynamic Coefficient	1.98E+01
S	Dimensionless number	
σ	Dimensionless number	
ω	Pump Speed (rad/s)	
D	Maximum Pump Displacement (m^3/rad)	
x	Percent of Maximum Displacement	

The values shown in Table 4 were found in the literature to generate efficiency maps that very closely matched the data presented in a 2004 EPA report (Shan, 2009). These pumps were designed specifically for testing that the EPA was conducting on hydraulic hybrids and are not commercially available. The intent of the design was to create a pump with a very high overall efficiency over a large operating region. The resulting efficiency maps can be seen in Figure 11. The efficiency maps were used in the simulation as a best case scenario since they were based upon data over the full operating range of the pump.

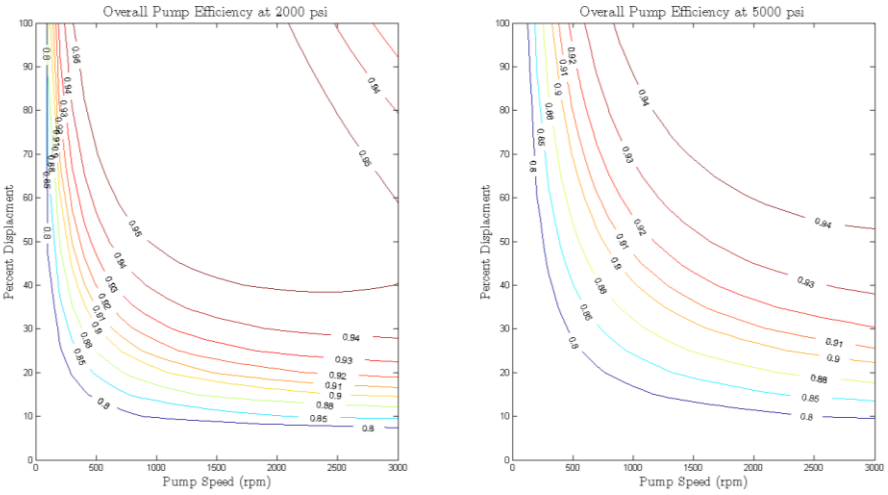

Figure 11. Estimated efficiency map of the bent axis pump presented in a 2004 EPA report.

The pump used in the Eaton system is a swash plate type, axial piston pump. The efficiency of this pump is expected to be lower than that of the bent axis pump discussed above. However, the values in Figure 11 were used as a starting point for further refinement of the pump efficiency.

The efficiency maps used to represent what was believed to be the actual pump were based on data from the Rexroth A4VSO pump. Data for this pump was used because performance data could not be found for a comparable Eaton pump. The A4VSO pump is a swash plate type, axial piston pump available in a wide range of sizes that are rated for 5075 psi (350 bar). Data for the 180 frame size of this pump series was used because it had a displacement of 11 in^3/rev (180 cc/rev) (Bosch Rexroth AG, 2011). The resulting efficiency maps can be seen Figure 12. The one limitation of this pump is that it is not rated for speeds up to 3000 rpm. However, there are not many pumps manufactured in this size range that can operate at this displacement. It is the belief of

the author that the pump used in the Eaton system is a variation of an existing Eaton pump design that has been thoroughly tested for this application.

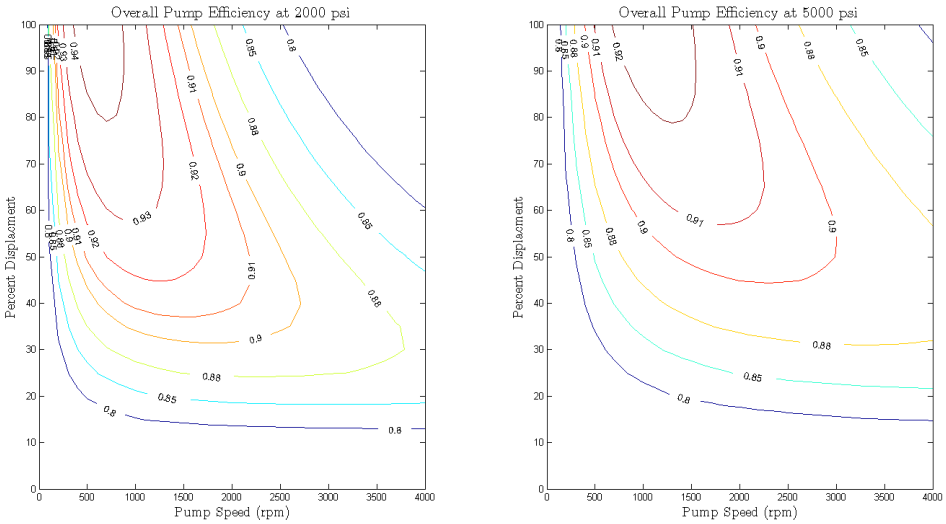

Figure 12. Estimated efficiency maps for the A4VSO piston pump.

The values that were used to generate the efficiency maps in Figure 12 are shown in Table 5. As a check for their validity they were compared to the constants presented for the bent axis pump in Table 4.

Table 5. Estimated constants used to predict the efficiency of the A4VSO piston pump.

Constant	Value
C_s	2.627×10^{-9}
C_{st}	1.332×10^{-7}
C_v	1.2×10^{-4}
C_f	0.021201
C_h	83.449

4.3 ACCUMULATOR MODEL

Two accumulator models were used for the different phases of the project. The use of either model was dictated by the how it was used in the code.

The first model assumed that the nitrogen behaved as an ideal gas, and its compression was assumed to be a polytropic process. This relation is shown in Equation 12 and was used for the development of the control policy for the vehicle because of the model's simplicity. More complex models could add more accuracy but would most likely involve differential equations which would add complexity and be difficult to implement in the derivation of the control policy because of the need for an additional state.

$$P_1 V_1^n = P_2 V_2^n \tag{12}$$

The decision to model the process as polytropic rather than isothermal or isentropic was made because in reality neither of these latter assumptions would occur. Even though the process may not be polytropic, it will most likely model the behavior of the gas more accurately because it is bracketed by the assumptions of the other two processes. Figure 13 depicts this behavior.

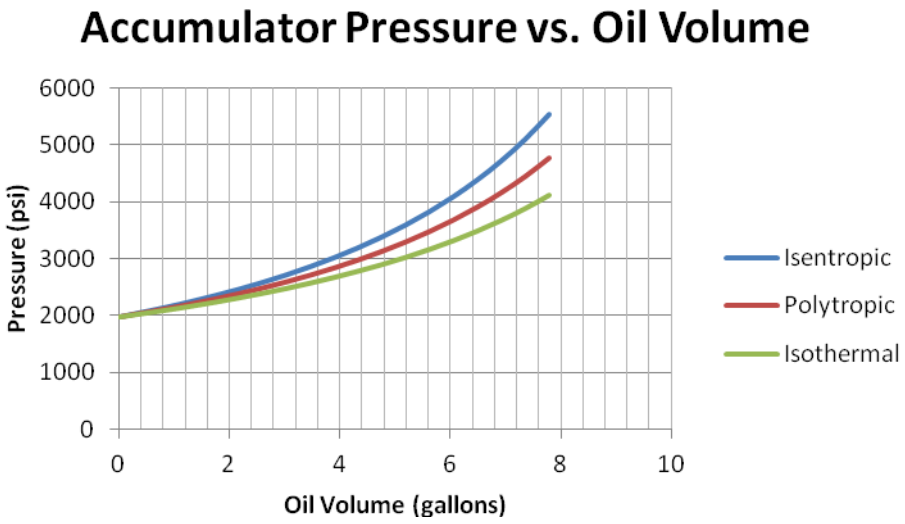

Figure 13. Pressure as a function of oil volume for a 15 gallon accumulator with various assumptions about gas behavior.

The second model was used in the simulation of the actual vehicle in Simulink. The decision to implement a more complex model was made because the rate at which the accumulator is filled or emptied will have an effect upon the behavior of the compression process. The accumulator being filled very rapidly may closely resemble an isentropic process while an isothermal process may better represent the accumulator being filled very slowly. There will also be heat transfer to and from the hydraulic oil. Even with no flow in or out of the accumulator this heat transfer will cause a change in the pressure.

The first difference for this model is to assume that the nitrogen behaves as a real gas. To predict this behavior, the Benedict-Webb-Rubin equation was used and is presented below as Equation 13. The constants used in this equation are presented in Table 6 (Cengel, 2001).

$$P = \frac{R_u T}{\bar{v}} + \left(B_0 R_u T - A_0 - \frac{C_0}{T^2} \right) \frac{1}{\bar{v}} + \frac{b R_u T - a}{\bar{v}} + \frac{a\alpha}{\bar{v}^6} + \frac{c}{\bar{v}^3 T^2} \left(1 + \frac{\gamma}{\bar{v}^2} \right) e^{-\gamma / \bar{v}^2} \qquad (13)$$

Table 6. Constants used with the Benedict-Webb-Rubin equation to predict real gas behavior of nitrogen (Cengel, 2001).

Constant	Value
a	2.54
A_o	106.73
b	0.002328
B_o	0.04074
c	7.379×10^4
C_o	8.164×10^5
α	1.272×10^{-4}
γ	0.0053

Otis and Pourmovahed (1985) analyzed a piston type accumulator by performing an energy balance and approximating the convective heat transfer by a single time constant. With these relations, a differential equation for the time derivative of gas temperature could be obtained. This relation is shown in Equation 14 where T_s is the wall temperature, T is the gas temperature, and τ is the time constant of the accumulator. One major difference that was made for this model was that T_s represents the wall of the rubber bladder. It was assumed that this bladder would stay at a constant temperature dictated by the hydraulic fluid. This temperature was assumed to be 110 °F.

$$\dot{T} = \frac{T_s - T}{\tau} - \frac{T}{c_v} \left(\frac{\partial p}{\partial T} \right)_v \dot{v} \qquad (14)$$

This equation is then combined with the partial derivative of the BWR equation with respect to temperature. This yields Equation 15 that can be implemented in the vehicle simulation.

$$\dot{T} = \frac{Ts - T}{\tau} - \frac{\dot{\bar{v}}}{c_v}\left[\frac{RT}{\bar{v}}\left(1 + b/\bar{v}^2\right) + \frac{1}{\bar{v}^2}\left(B_o RT + 2C_o/T^2\right) - \frac{2c}{\bar{v}^3 T^2}\left(1 + \frac{\gamma}{\bar{v}^2}\right)e^{-\gamma/\bar{v}^2}\right] \quad (15)$$

However, the time constant must still be found for this particular accumulator. It was also noted that the specific heat at constant volume should be corrected for changes in temperature and pressure. Rather than correct the specific heat as discussed by Otis and Pourmovahed, data was downloaded from the NIST Chemistry WebBook for the entire operating range of the gas (National Institute of Standards and Technology, 2011).

There are several methods for determining the time constant of an accumulator. These include both analytical and experimental methods. Because hardware was not available to test, an analytical method was used.

The method chosen was also used to analyze a piston type accumulator. Therefore some modifications were made to the method that was presented to approximate a bladder type accumulator. The assumptions made by this method were.

1. The average temperature distribution in the gas with convection approximates that of a solid with conduction only.
2. The walls of the accumulator are maintained at a constant temperature.
3. The density of the gas remains constant during heat transfer and all changes in density occur adiabatically.

The final relation that was derived for the time constant with these assumption is presented in Equation 16. In order to calculate the time constant, an effective diffusivity must also be calculated, which involves calculating the Prandtl and Grashof numbers. The derived Grashof number is presented in Equation 18, and the effective thermal diffusivity was calculated using Equations 17 and 18 (Svoboda, Bouchard, & Katz, 1978). To calculate these numbers the dynamic viscosity, specific heat at constant pressure, specific heat at constant volume, and thermal conductivity from the NIST database were used in lookup tables rather assume constant values (National Institute of Standards and Technology, 2011).

$$\tau = \frac{0.428R^2(L/D)}{\alpha_e(2+4(L/D))} \tag{16}$$

$$\alpha_e = 0.23(Gr * \Pr)^{1/4}\alpha_o \tag{17}$$

$$Gr = \frac{2g\ \delta^3\left\{1-\left[(p_o+p_s)/(p_i+p_s)\right]^{\gamma-1}\right\}}{\left[\nu_s p_s/(p_o+p_s)\right]^2\left\{1+\left[(p_o+p_s)/(p_i+p_s)\right]^{\gamma-1}\right\}} \tag{18}$$

The dimensions for the accumulator were taken from the Eaton specification sheet and are presented in Table 7. A cross section of the accumulator and a drawing depicting the various dimensions can be seen in Figure 14 (Eaton Corporation, 2005).

Table 7. Dimensions of the bladder accumulator used in the present vehicle simulation (Eaton Corporation, 2005).

Feature	Dimension
Assembly length (A)	78.8” (2002 mm)
Connection Length (B)	5.5” (140 mm)
Gas Valve Length (C)	2.8” (70 mm)
Diameter (D)	9.1” (232 mm)

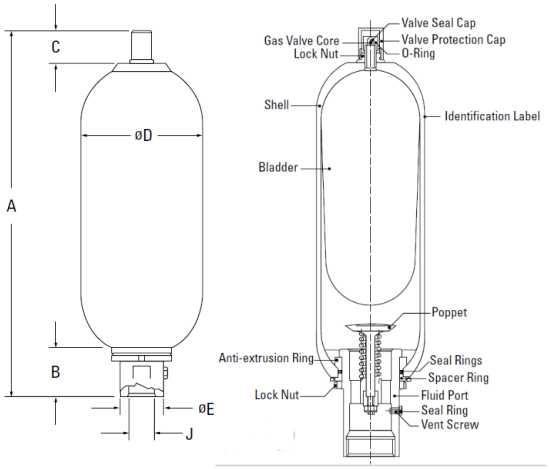

Figure 14. Cross section of a bladder type accumulator and labeled dimensions corresponding to values in Table 7 (Eaton Corporation, 2005).

In order to use this model, a few modifications were made to predict the behavior of this specific accumulator. The first thing to note is that the diameter was assumed to be 90% of the outside diameter listed in the specification sheet. This was done for two reasons. The first is that the wall will account for a portion of the diameter. The second is that the bladder is tapered which allows for some space between the bladder and the wall. This can be seen in Figure 14. The volume of the spherical ends of the bladder

were ignored, and the gas was assumed to be in the shape of a cylinder. This allowed for the characteristic length to be easily estimated.

The resulting plots shown in Figure 15, Figure 16, and Figure 17 depict how the flow rate into the accumulator affects the pressure and temperature of the system. Both traces pump a total of 7 gallons of fluid into the accumulator at the specified flow rate. After the fluid has been put into the accumulator, it is allowed to sit and allows the nitrogen gas to reach a thermal equilibrium at constant volume. This condition could occur as a vehicle decelerates to a stop and then idles.

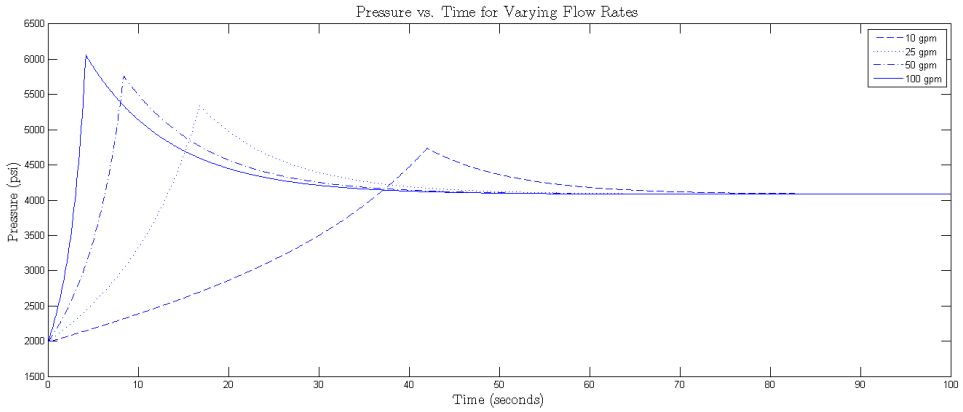

Figure 15. Pressure vs. time of an accumulator being filled with 7 gallons or fluid at varying rates.

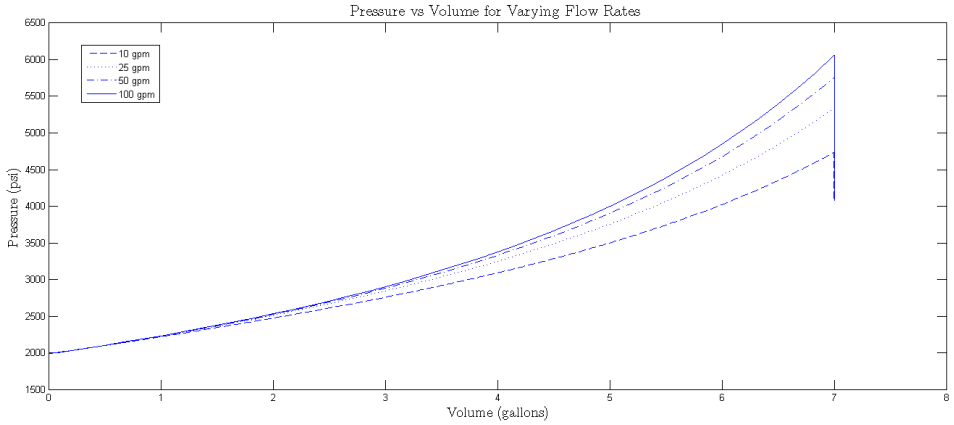

Figure 16. Pressure vs. oil volume of an accumulator being filled with 7 gallons or fluid at varying rates.

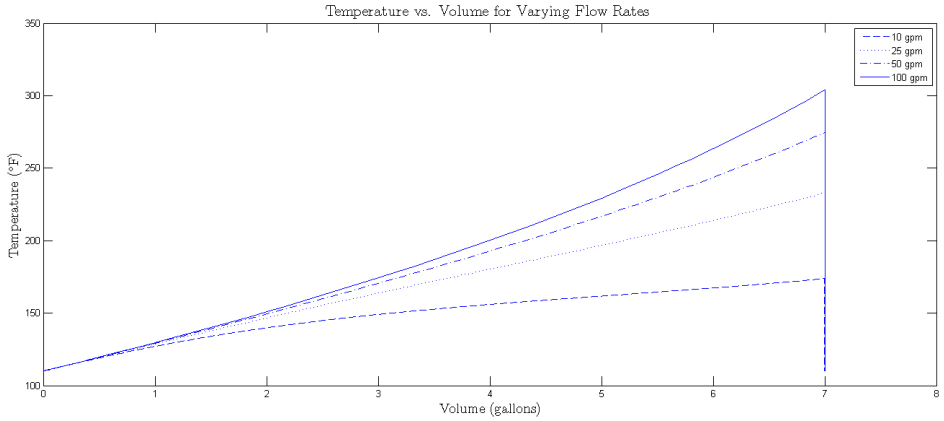

Figure 17. Temperature vs. time of an accumulator being filled with 7 gallons or fluid at varying rates.

There are several points to note about these plots and how they may differ from actual vehicle operation. The first is that the maximum pressure reached in the accumulator will be 5000 psi because of either the control strategy or a relief valve within the system. The peaks above this level occurred in these plots because the same amount of fluid was added each time to keep conditions somewhat constant. The peak

temperature of 350 °F will most likely not occur in the system because the gas will not be compressed to 6000 psi.

4.4 Transfer Case

The transfer case is responsible for connecting the pump to the drivetrain of the vehicle. Based on information from the service manual, it is known that the pump has a maximum speed of 3000 rpm and it is disengaged at a vehicle speed of 24 to 26 mph (Eaton Corporation, 2011d).

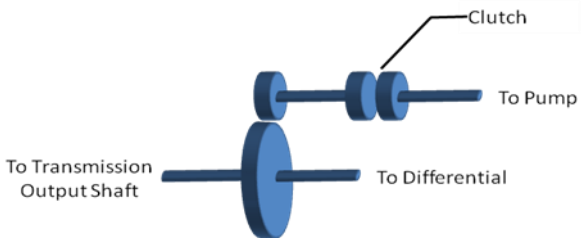

Figure 18. Representation of transfer case used to connect the pump to the drivetrain.

The image presented in Figure 18 is a basic representation of the transfer case. The ratio was selected to have the pump reach its maximum speed at 25 mph when it is disengaged. This was found using Equation 19.

$$R_{tc} = \frac{R_{tire}\omega_{\max\ pump}}{R_{diff}V} \tag{19}$$

There will be some losses that occur within the transfer case as power is transferred to and from the hybrid system. The losses that occur as power is transferred from the transmission to the differential were neglected as they will only include losses due to bearings and seals. The main loss for concern within this component is the gear

pair. Two separate models were used to estimate this efficiency. The first method was to assume a constant 95% efficiency. This was used in the development of the control strategy because of its simplicity.

$$\tau_{out} = \tau_{trans} + \tau_{pump} R_{tc} \eta_{tc}^{\mathrm{sgn}(\tau_{pump}\omega_{pump})} \tag{20}$$

The 2nd method attempts to capture the losses that vary with torque and speed. This method simply used a generic manual transmission model to estimate the efficiency of the transmission. This method will include estimates for losses caused by gear pair losses, windage, seal drag, and bearing losses for a manual transmission (R. D. Matthews et al., 2011). Since the exact configuration of the gear box is unknown, it is not possible to make an exact estimate. Therefore, it was assumed that the manual transmission model would yield a representative estimate. Figure 19 shows the estimated efficiency of the gear box predicted by this model.

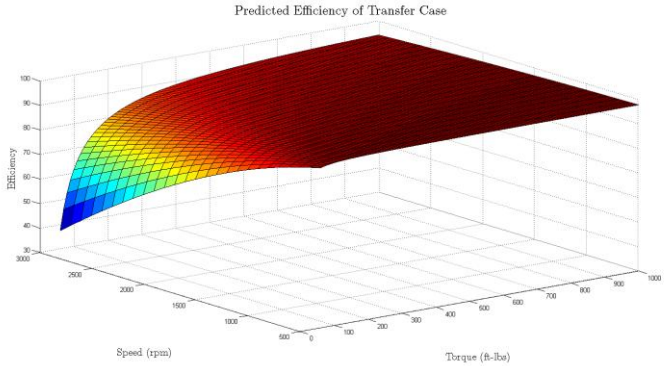

Figure 19. Predicted efficiency of the transfer case used with the modeled hybrid system.

4.5 HOSE LOSSES

The losses within hoses were modeled as pipe flow. No distinction was made between hoses and tubes. It was assumed that the slight differences in diameter would be

negligible. A general rule of thumb is that the results will be within 10% when modeling turbulent flow (Munson, Young, & Okiishi, 2001). Adding additional complexity may not generate more accurate results.

In order for the hose pressure drop to be easily included in the model, the pressure drop per foot of hose length was calculated. This was done using the Darcy-Weisbach Equation shown in Equation 21 (Munson et al., 2001).

$$\Delta p = f \frac{l}{D} \frac{V^2}{2g} \tag{21}$$

Laminar flow was assumed to occur with a Reynolds number less than 2100, and turbulent flow was assumed to occur with a Reynolds number above 4000 (Munson et al., 2001). For Reynolds numbers between these two values, the friction factor (*f*) was interpolated between the upper bound of laminar flow and the lower bound for turbulent flow. The friction factor for laminar flow was estimated using Equation 22.

$$f = \frac{64}{\mathrm{Re}} \tag{22}$$

The process for estimating the friction factor for turbulent flow was more involved. The Colebrook Equation was used to estimate this parameter and is shown in Equation 23 (Munson et al., 2001). Because this equation cannot be solved algebraically, it was solved numerically at each operating point to estimate the pressure drop per foot of hose.

$$\frac{1}{\sqrt{f}} = -2.0\log\left(\frac{\varepsilon/D}{3.7} + \frac{2.51}{\mathrm{Re}\sqrt{f}}\right) \tag{23}$$

Table 8. Parameters used for estimating pressure drop in hoses and tubes (Esposito, 2003; Manring, 2005).

Parameter	Value
Dynamic Viscosity (μ)	11.3 cP
Specific Gravity	0.84
Relative Roughness	0.00006 in

The results were verified against the data found in the "Fluid Power Designers' Lightning Reference Handbook" and were found to very closely agree (Berendsen Fluid Power, Inc., 1990). The results for several diameters of hose are shown in Figure 20.

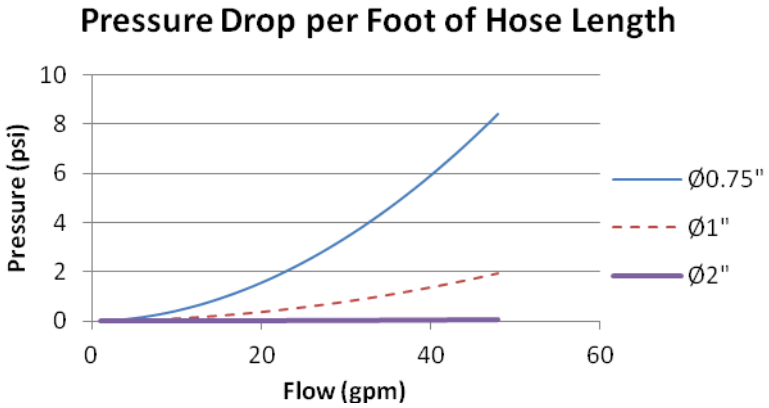

Figure 20. Estimated pressure drop per foot for several diameters of hose.

The diameters for the various hoses in the hybrid system were taken directly from the service manual for the system. However, the lengths were estimated. These values are shown in

Table 9. The suction tube on the pump was not considered as a potential for loss because it will be sized very large to reduce pressure drop and prevent cavitation.

Table 9. Diameter and estimated lengths of hoses used in the modeled hybrid system (Eaton Corporation, 2011d).

Hose	Length	Size
Cooler Inlet	3’	-16 (1”)
Cooler Outlet	3’	-16 (1”)
Pump to Accumulator	2’	-24 (1 ½”)
Return	2’	-32 (2”)

4.6 Refuse Body Hydraulic Circuit

The refuse body requires a hydraulic circuit for its operation. As mentioned earlier, the system has a gear pump mounted directly to the engine. Based on the refuse body specification sheet, the pump is rate for 42 gpm at 1200 rpm. The selected pump has a displacement of 8.94 in^3/rev with a maximum operating pressure of 2500 psi.

The volumetric efficiency of this pump was estimated based off of the data presented in its specification sheet (Geartek, 2008). The pump flow as a function of speed is shown in Figure 10 and is presented in Chapter 3. The efficiency of the pump was estimated based on that data. No attempt was made to use the efficiency model presented for the hybrid pump to predict the effect pressure may have on the efficiency. Use of that model would have added complexity to the system, and pressure does not have a large effect on efficiency based on the graphs shown in that section.

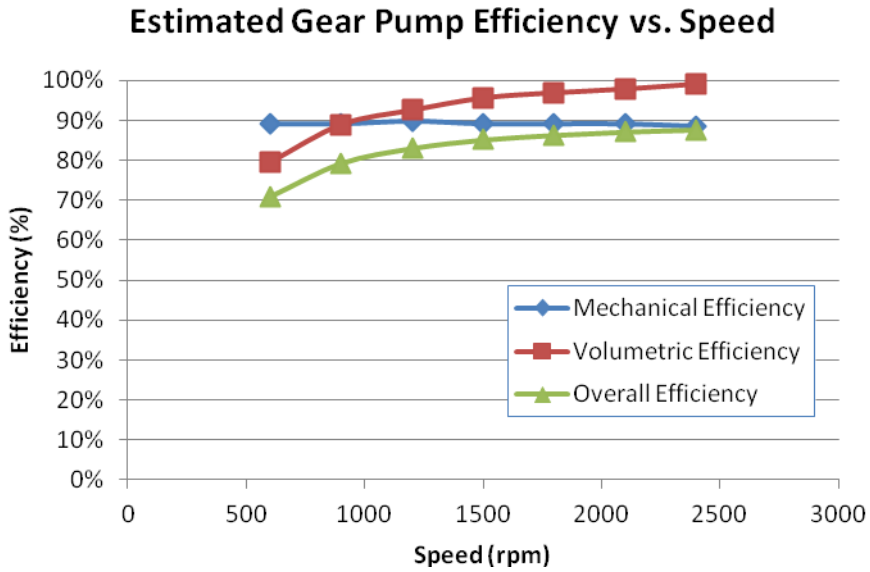

Figure 21. Estimated gear pump efficiency based on data from the pump specification sheet (Geartek, 2008).

With the estimated efficiency of the pump now known, the flow can be calculated based upon engine speed. The open center pressure drop of the system can then be calculated based on this flow. A brief schematic of the system is presented in Figure 22. Because all of the components are in series, the pressure drop across each element directly adds. The open center pressure drop for the components as a function of flow can be seen in Figure 23.

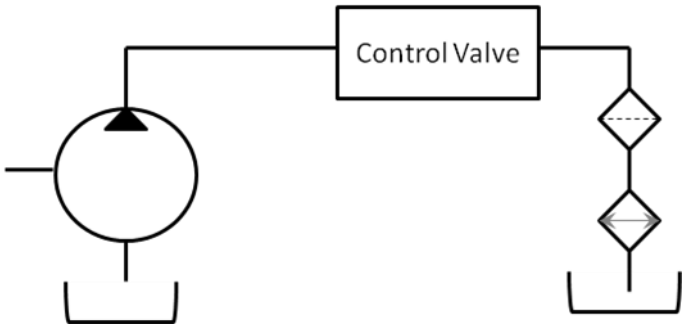

Figure 22. Schematic of the hydraulic circuit for the refuse body.

The component responsible for the largest pressure drop is the control valve. This is due to the fact that the fluid must flow through many passages to get through the valve. The valve selected for this application was a Muncie 90V Series valve. This valve is a sectional open center valve. The pressure drop data was taken directly from the specification sheet for a 3 section valve.

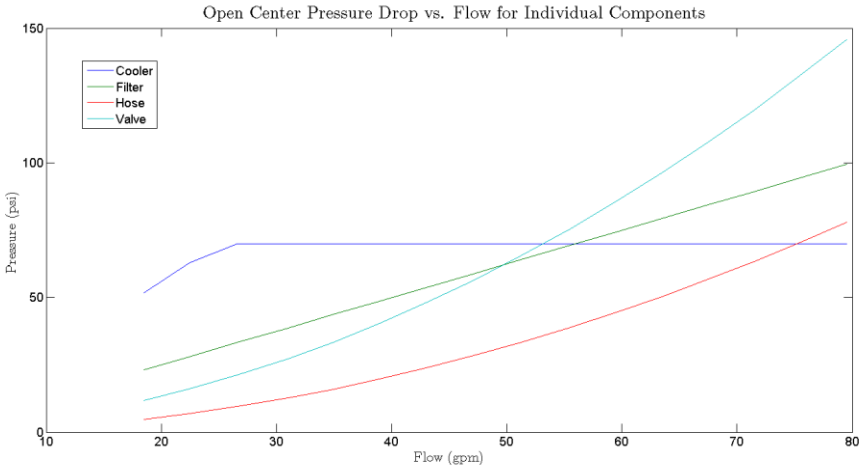

Figure 23. Open center pressure drop of various components in the refuse body hydraulic circuit.

Other components that were included in the system were a heat exchanger, filter, and hoses. The hoses were assumed to be 1" in diameter with a total combined length of 15'. The filter was assumed to have a pressure drop of 100 psi at 80 gpm. The heat exchanger was slightly more complicated. It was assumed to have a pressure drop of 70 psi at a flow of 25 gpm. Below this level of flow, the pressure drop across the heat exchanger is regulated by the flow through the heat exchanger. Above this flow the pressure is regulated to 70 psi by a check valve in parallel with the heat exchanger. This is done to limit the maximum pressure experienced by the heat exchanger to prevent damage. This also allows for a smaller heat exchanger to be used which reduces cost. A plot of the assumed pressure drop for all of these components can be seen in Figure 23.

With the estimated pressure drop for the entire system, the torque requirement of the pump can be estimated as a function of engine speed. This data is presented in Figure 24 along with the corresponding power requirement. This load could be reduced by resizing of components or changing the architecture of the system. However, it was modeled this way to mimic what is used in reality.

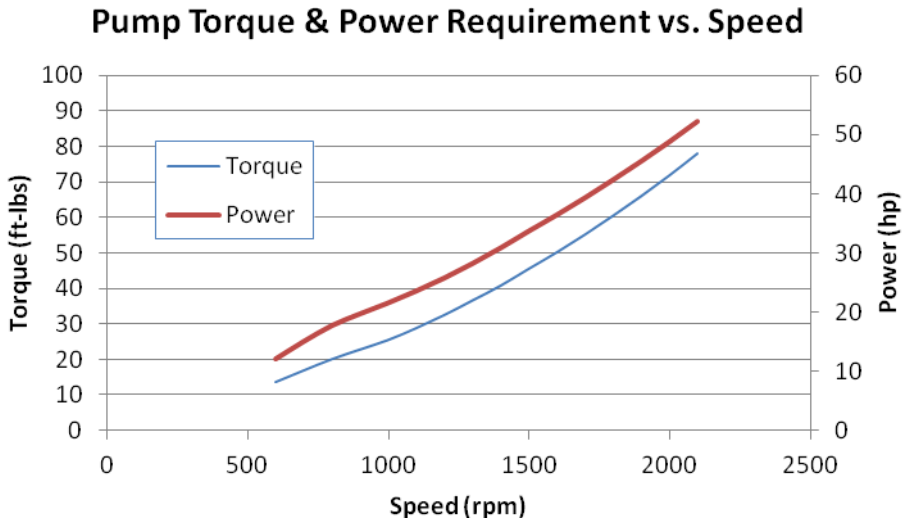

Figure 24. Estimated torque and power requirement of the hydraulic system pump.

It is also important to note that the load of the hydraulic system functioning was not included in this model. It was assumed that the load would only occur while the vehicle was at rest. During this time the hybrid system could not function. Therefore, this load should be a constant difference in the amount of fuel consumed that could be added to the estimated fuel usage from the simulation.

4.7 Control Strategy

The control strategy that was implemented was based heavily on the work of Lin and coworkers (2004) who developed a similar strategy for a parallel electric hybrid truck

with a very similar layout. In general, the process presented in their work was used with some deviations based on ease of implementation and differences in the system (Chan-Chiao Lin et al., 2004). This method was chosen based on its ability to be trained over several drive cycles and no need for curve fitting to estimate the optimal policy.

The first step of the process was to model the driver power demand as a stochastic process. For this implementation, the vehicle speed was also assumed to be stochastic. In previous work, the vehicle speed was assumed to be deterministic (Chan-Chiao Lin et al., 2004). However, this was not assumed in this case because there was no advantage in assuming that the process was deterministic based on the way the code was written for later steps in the process.

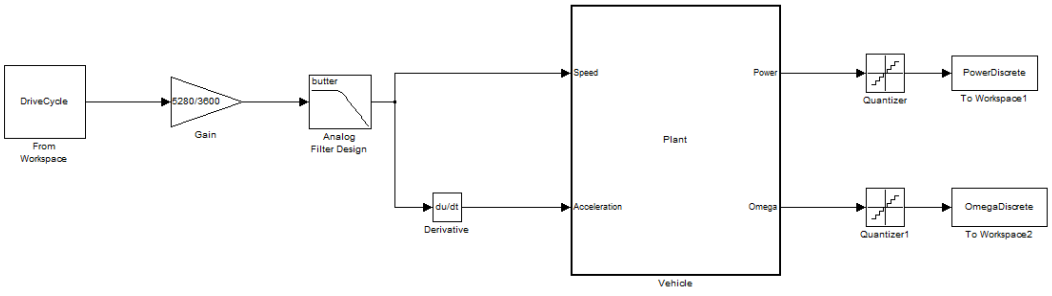

Figure 25. Simulink diagram of the model used to estimate driver power demand over various drive cycles.

In order to calculate the power demand of the vehicle a model was constructed that evaluated the derivative of the drive cycle to estimate the required power demand. This is shown in Figure 25. A 3rd order butterworth filter was used to guarantee that the derivative of the drive cycle was smooth. The initial cutoff frequency of the filter was set at 0.5 Hz because the drive cycle data was given at a sample rate of 1 Hz. This was a logical way to initially set the cutoff frequency based on the Nyquist rate. This was the

method was initially thought to be acceptable by performing a fast Fourier transform on several drive cycles which included the Central Business District, Manhattan, New York Garbage Truck, New York Truck, Orange County Bus, West Virginia University City, and Heavy Duty Urban Dynamometer Driving Schedule cycles. These results are presented in Figure 26. However, this proved to be an unacceptable method because the maximum power requirement, where sharp changes in the drive cycle occur, were being omitted. The final cutoff frequency used was 100 rad/s based on trial and error. This value may also be dependent upon the behavior of the model used for the driver.

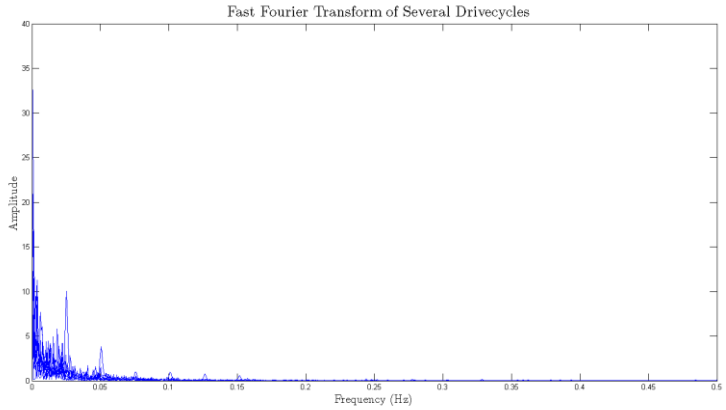

Figure 26. Fast Fourier transform of several drive cycles for verification of the filter cutoff frequency.

$$\tau_{wheel} = \frac{m_{eff} a + F_{drag} + F_{roll}}{R_{tire}} \tag{24}$$

$$P_{dem} = \tau_{wheel} \omega_{wheel} \tag{25}$$

With Equations 24 and 25, the power can be estimated and discretized for later steps. The discretization of the variables at this step has a direct impact on the size of the

problem that is formally defined in later steps. A fixed step solver was used for this step because it allowed for the data to be easily downsampled to 1 Hz.

This data is then used to compute the transition probability matrix, which is the probability of the next state based on the current state of the vehicle. A visual representation of the computed transition probability matrix is shown in Figure 27. Because the states for this particular problem are power demand and wheel speed pairs, the numerals on the X and Y axes have no exact physical meaning. They are just the number assigned to a particular state. However, the lower state numbers correspond to lower power demand combinations while the higher state numbers correspond to larger power demands.

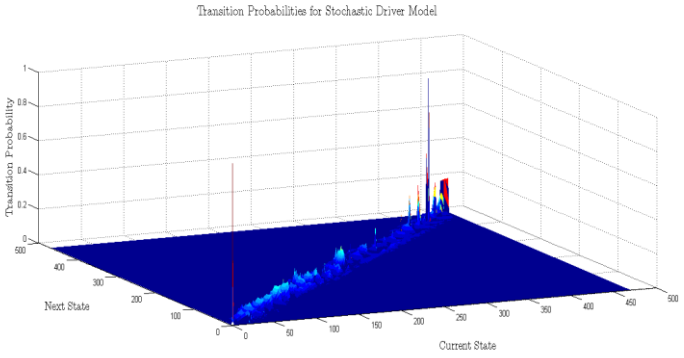

Figure 27. Visual representation of the transition probability matrix used to develop a Markov Chain of driver power demand and vehicle speed.

To begin the process of formally defining the Markov chain, the power demand and wheel speed are discretized as shown below. The sets of these values include the potential range of values that they may take and are defined in Equations 26 and 27. The complete state vector is defined as *S* in Equations 28 and 29. This will later be augmented to include system pressure.

$$P_{dem} \in \left\{P_{dem}^1, P_{dem}^2, P_{dem}^3, \ldots, P_{dem}^N\right\} \tag{26}$$

$$\omega_{wheel} \in \left\{\omega_{wheel}^1, \omega_{wheel}^2, \omega_{wheel}^3, \ldots, \omega_{wheel}^N\right\} \tag{27}$$

$$s \in S \tag{28}$$

$$s = (P_{dem}^i, \omega_{wheel}^i) \tag{29}$$

The transition probability was estimated based on standardized drive cycles that included the HUDDS, Manhattan Cycle, New York Truck Cycle, and the Orange County Bus Cycle. The equation used to estimate this value is shown below in Equation 30. The variable m_{ij} represents the number of transitions from state i to state j, and m_i is the total number of visits to state i. It is also important to note the constraint given in Equation 31 that the sum of the transition probabilities for a state i must equal 1 (Chan-Chiao Lin et al., 2004).

$$\hat{p}_{ij} = \frac{m_{ij}}{m_i} \tag{30}$$

$$\sum_{j=1}^{n} p_{ij} = 1 \tag{31}$$

Using the data that has been derived from the drive cycles with the basic vehicle model, an optimal policy can then be found by formulating the problem as a Markov decision process. The method chosen to derive this policy is referred to as policy iteration and was chosen based on previous work (Chan-Chiao Lin et al., 2004). This

particular method is a dynamic programming type algorithm and does have some issues. The two main issues are that they are computationally intense and assume a perfect model (Sutton & Barto, 1998, p. 89).

The first step of this phase is to define a set of states (S) and a set of actions ($A(s)$). The set of states, S, is an augmented version of the set defined previously. The definition now includes the discretized accumulator pressure so that the complete set includes all possible combinations of wheel speed (ω_{wheel}), power demand (P_{dem}), and accumulator pressure (P_{acc}). The set of actions, $A(s)$, was defined as all possible combinations of transmission gear (R_{trans}) and the "power split ratio (PSR)", which is defined in Equation 34. When this value is 0, the vehicle is being driven entirely by the hybrid system. However, when it is 1, it is being powered entirely by the engine. Values less than one indicate a blending of power to meet demand while values larger than one indicate charging of the hydraulic accumulator while still meeting the power demand.

$$P_{acc} \in \left\{P_{acc}^1, P_{acc}^2, P_{acc}^3, \ldots, P_{acc}^N\right\} \tag{32}$$

$$s = (P_{dem}^i, \omega_{wheel}^i, P_{acc}^i) \tag{33}$$

$$PSR = \frac{P_{eng}}{P_{dem}} \tag{34}$$

Since the accumulator pressure is based on a deterministic process, it can be calculated with the current state and action taken to determine the transition probabilities for the next state. The compression of the accumulator charge was treated as a polytropic process for this step using Equation 12 in the section describing the accumulator model.

The next step is to determine the cost function to optimize the control policy against. The cost function in this case was fuel consumption (m_{fuel}), but it is not limited to this. Other factors, such as vehicle emissions or deviation from a particular accumulator charge, could be included in the cost function. The formal definition of the cost function is shown in Equation 35. The variable γ is the discount rate that determines the weight of future fuel consumption. It must be greater than or equal to 0 but less than 1.

$$J = m_{fuel,t+1} + \gamma\, m_{fuel,t+2} + \gamma^2 m_{fuel,t+3} + \ldots = \sum_{k=0}^{\infty} \gamma^k m_{fuel,t+k+1}$$
$$0 \le \gamma < 1 \tag{35}$$

Constraints must also be placed upon the optimization so that the system will be operated in a way that is acceptable. These constraints include engine speed, engine torque, pump displacement, and accumulator pressure. The inequalities below represent these constraints. Pump speed was not included as a constraint because it was assumed to be disengaged at 25 mph automatically to prevent the maximum pump speed from being exceeded. This was based on information from the service manual.

$$\omega_{eng,\min} \le \omega_{eng,k} \le \omega_{eng,\max} \tag{36}$$

$$\tau_{eng,\min} \le \tau_{eng,k} \le \tau_{eng,\max} \tag{37}$$

$$D_{pump,\min} \le D_{pump,k} \le D_{pump,\max} \tag{38}$$

$$P_{acc,\min} \le P_{acc,k} \le P_{acc,\max} \tag{39}$$

The method used to solve this problem is known as policy iteration. This method consists of two stages which are policy evaluation and policy improvement (Sutton & Barto, 1998). During the policy evaluation step, estimates for the "state value function" (V^{π}) are estimated based on the current policy (π). The state value function is the cost associated with a given policy. For the first iteration an arbitrary policy is used. However, for subsequent iterations the policy developed in the policy improvement step is used. During the policy improvement step a new and improved policy (π') is estimated based on the current estimate of V^{π} for each state. By iterating through these two steps an optimal policy (π^{*}) is found.

$$J_i = m_{fuel}(s_i, \pi(i)) + \gamma \sum_{j=1}^{n} p_{ij}(\pi(s_i)) J_j \tag{40}$$

In order to estimate V^{π}, the cost function shown in Equation 35 is combined with the transition probabilities to form Equation 40. This equation represents the most probable cost that will be incurred based on the current state. The terms J_i and J_j denote the costs associated with the current state i and the next visited state j. This equation can then be manipulated algebraically to yield a set of linear equations which can be solved to find the cost of each state J to yield V^{π}. This is shown in Equation 41. The lsqr function in MATLAB was used to solve for these values to avoid issues with the inversion of a sparse matrix.

$$\begin{bmatrix} 1-p_{11} & p_{12} & \cdots & p_{1n} \\ p_{21} & 1-p_{22} & \cdots & p_{2n} \\ \vdots & \vdots & \ddots & \vdots \\ p_{n1} & p_{n2} & \cdots & 1-p_{nn} \end{bmatrix} \begin{bmatrix} J_1 \\ J_2 \\ \vdots \\ J_n \end{bmatrix} = \begin{bmatrix} m_{fuel}(s_1, \pi(s_2)) \\ m_{fuel}(s_2, \pi(s_2)) \\ \vdots \\ m_{fuel}(s_n, \pi(s_n)) \end{bmatrix} \tag{41}$$

With the data found in policy evaluation, the policy improvement step can now be completed. This is accomplished using Equation 42 which estimates the cost J_i with the estimated costs from the previous step. The action that yields the minimum cost is chosen for each state to develop the next iteration of the policy π. This iteration process continues until the policy stabilizes.

$$\pi(s_i) = \arg\min_{a \in A(s)} \left[m_{fuel}(s_i, a) + \gamma \sum_{j=1}^{n} p_{ij}(a) J_j \right] \tag{42}$$

A portion of the resulting policy for power split ratio is shown in Figure 28. A corresponding gear shift map is not shown because it is in a constant gear at this speed regardless of power demand or system pressure. The portion shown represents the policy for the power split ratio at a given wheel speed of 6 rad/s. Additional layers of the policy exist for each speed from 0 rad/s to 52 rad/s. When implemented within the simulation, a nearest neighbor interpolation is used to find the specified action for the state of the vehicle.

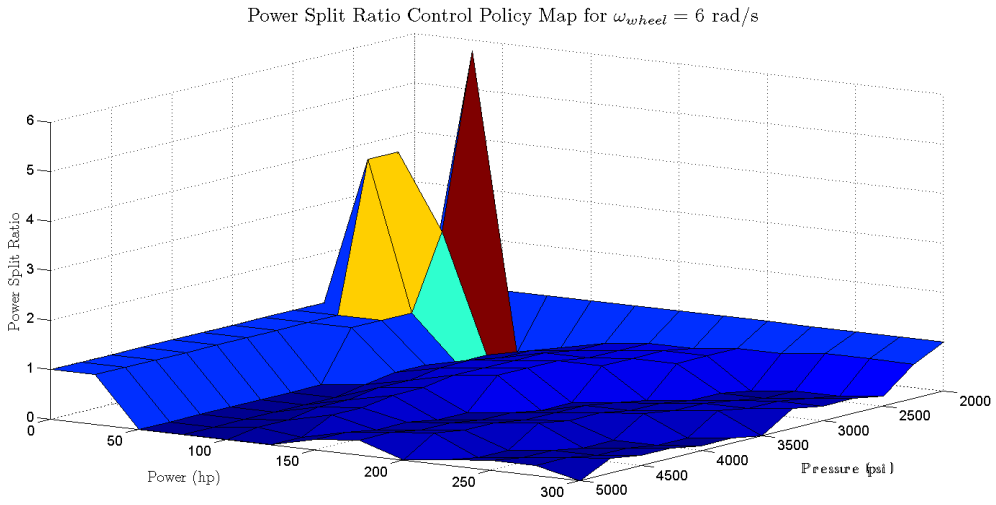

Figure 28. Power split ratio map for a wheel speed of 6 rad/s.

Chapter 5: Vehicle Simulation and Results

The refuse truck was simulated through several standardized driving cycles that meant to replicate actual conditions. These cycles were chosen to analyze the vehicle under a wide range of conditions that would demonstrate how the system may perform whether good or bad. The method used to simulate the vehicle and predict the fuel economy was developed to eliminate any bias due to the initial and final states of accumulator charge.

5.1 SIMULATION METHOD

When simulating a hybrid vehicle it is important to ensure that the initial charge of the energy storage device does not bias the results by having a different final energy level. The typical method used for electric hybrids is to ensure that the initial and final states of charge are identical. Figure 29 demonstrates the effect of the initial pressure on the resulting fuel economy for three different cycles. The percent increase in this figure is the percentage increase from the base value when the accumulator is initially empty.

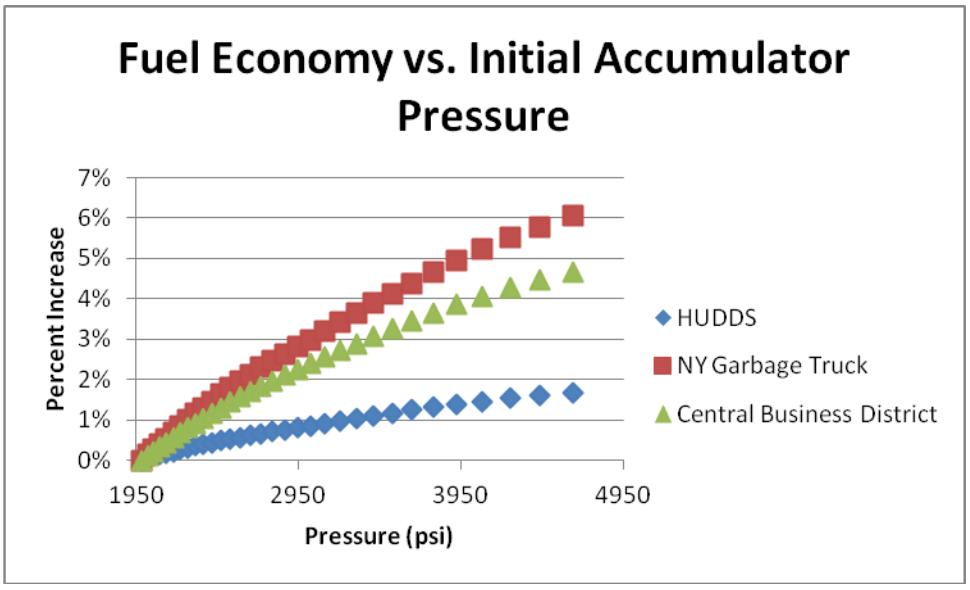

Figure 29. Effect of initial accumulator charge on fuel economy for various drive cycles.

This method works very well for electric hybrids because the energy level of the battery is defined by the SOC for a simple resistive model, and the same methodology can easily be used for a hydraulic hybrid when the nitrogen charge in the accumulator is treated as an ideal gas. This is because a given pressure always corresponds to a given volume and is path independent. However, the modeling of the temperature and heat transfer of the accumulator presents an issue. The final energy level of the accumulator can be defined as the enthalpy of the nitrogen which is function of both the temperature and volume of the nitrogen. This value is also time dependent and is based on how long the vehicle idles at the end of the drive cycle. An alternative to this procedure would be to ensure the initial and final volumes of the accumulator were identical. This would give an equivalent energy level assuming identical temperatures before and after the cycle if the vehicle idles long enough.

Rather than choosing between fluid level or enthalpy an alternative method was used. This method was to simply simulate the vehicle through the drive cycle multiple times continuously. This makes the deviation in the energy level of the accumulator insignificant in relation to the total energy required to propel the vehicle for the cycle. It also eliminates the need to simulate the vehicle several times to match the initial and final energy levels, which makes it very easy to run batch simulations. However, this would not be as feasible for an electric hybrid because of its larger energy capacity and a limitation on the maximum battery current. The Eaton electric hybrid system used by UPS and Coca-Cola has a battery rated for 1.8kW-hr, and a motor rated for a maximum of 44 kW (59 hp) (Lammert & (US), 2009; National Renewable Energy Laboratory, 2011). The accumulator used in this system was estimated to have an energy capacity of about 0.5 kW-hr. This estimate assumes that the accumulator contains 287 moles of diatomic nitrogen, a temperature of 110 °F, a precharge of 1985 psi, and a maximum pressure of 5000 psi.

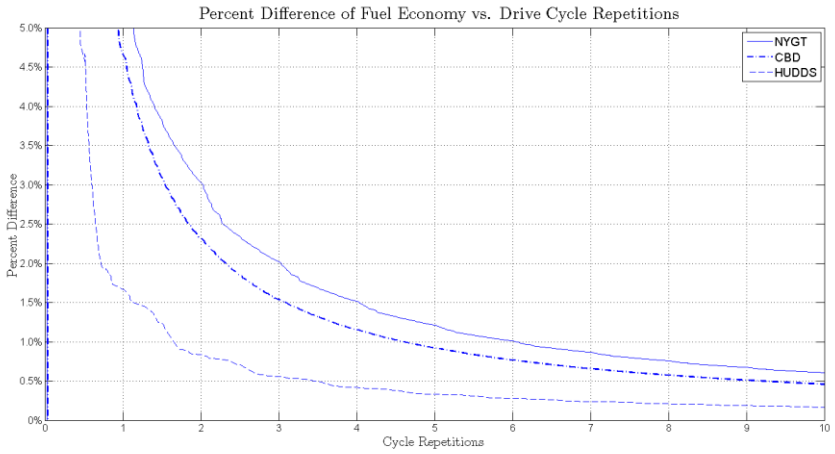

Figure 30. Percent difference in fuel economy based on initial state of accumulator as a function of drive cycle repetitions.

The chart shown in Figure 30 depicts the percent difference in the fuel economy between an initially empty accumulator and an accumulator that is initially full. The convergence is somewhat dependent on the drive cycle, but it does converge. Based on the results shown in the chart, a total of 10 repetitions were conducted for each drive cycle to be confident that the error would be below 1%. The extra repetitions were added because there was some deviation between drive cycles. The initial charge of the accumulator is also given an initial oil volume of 5 gallons for all subsequent simulations to help minimize this deviation.

5.2 VEHICLE SIMULATION SENSITIVITY

Several vehicle configurations were simulated to help determine how different factors affected the results. The parameters that were analyzed included the pump efficiency, accessory loads, estimated accumulator time constant, and transmission configuration.

5.2.1 Pump Efficiency Sensitivity

The efficiency map of the pump was a source of uncertainty in the model. While actual test data was available for the EPA pump, it may not be representative of the actual pump. The actual pump is believed to perform similar to other commercially available piston pumps. The simulation was run with both efficiency maps presented in Chapter 4 to determine how sensitive the model may be to this parameter.

The simulations used to analyze the impact of pump efficiency were run with a vehicle weight of 56,000 lb. This weight was used because this condition would provide the most potential for improvement for the hybrid system. With a larger improvement in fuel economy, any impact the pump may have would be more noticeable. The other parameter that was varied was the accessory loads. One condition used only the assumed

loads of the air brakes, air conditioner, power steering, and cooling fans. The other condition included only the load from the refuse body hydraulic system. The second condition is not realistic, but was done to improve the fuel economy and provide a different set of conditions to evaluate the impact of pump efficiency. The accessory loads are very important when a large amount of time is spent idling and there is not a large amount of energy spent to propel the vehicle.

The results for the various simulations are presented below in Table 10 and Table 11. These tables present fuel economies and the percent improvement of the bent axis pump. Based on these results the high efficiency pump does not provide a huge benefit for this application with the largest increase only being 0.5%. However, more analysis was conducted to better understand if the system somehow compensated for the change in efficiency. This is possible because different control policies were developed for either pump.

Table 10. Simulation results that evaluate impact of pump efficiency maps with only accessory loads.

	High Efficiency Bent Axis Pump	Swash Plate Type Pump	Percent Improvement
NY Truck	4.52	4.51	0.2%
HUDDS	7.92	7.91	0.1%
NY Garbage Truck	2.98	2.98	0.1%
Orange Country Bus	6.61	6.61	0.1%
WVU City	5.59	5.58	0.3%
CBD	7.29	7.29	0.1%

Table 11. Simulation results that evaluate the impact of pump efficiency that neglect accessory loads and includes the refuse body hydraulic system load.

	High Efficiency Bent Axis Pump	Swash Plate Type Pump	Percent Improvement
NY Truck	8.05	8.02	0.4%
HUDDS	10.24	10.23	0.1%
NY Garbage Truck	8.14	8.11	0.3%
Orange Country Bus	9.75	9.73	0.2%
WVU City	9.98	9.93	0.5%
CBD	11.62	11.60	0.2%

To further investigate the effect of the impact of the pump efficiency, the system was analyzed during the first 55 seconds of the CBD cycle. The three model parameters that were used to understand the pump behavior were the oil volume in the accumulator, the pump displacement, and the overall pump efficiency. Despite the fact that the fuel economy was much the same, the operation did deviate some to compensate for the difference in efficiency.

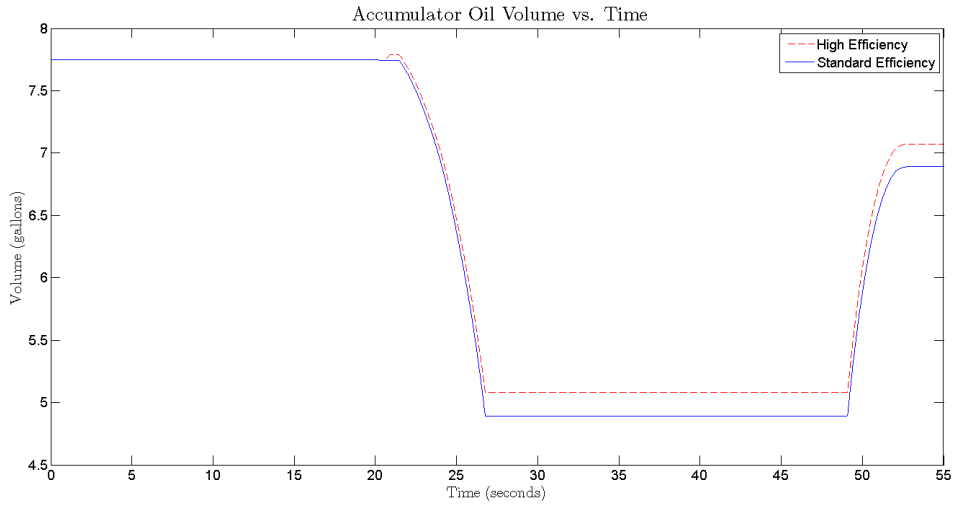

Figure 31. A Comparison of the accumulator volume for the two evaluated pump efficiency maps during the first 55 seconds of ten CBD drive cycle.

The plot of accumulator volume shown in Figure 31 does show that the standard efficiency pump requires more fluid to accelerate the vehicle, the high efficiency pump is operated slightly different than the standard efficiency pump. During the period of acceleration that begins about 20 seconds into the simulation, both pumps provide the same level of torque. The one exception is the one "jog" shortly after the acceleration begins where the engine is loaded by the high efficiency pump. To confirm why these differences occurred, the displacement was plotted. It verified that a larger displacement of the standard pump was required to generate the same torque. This can be seen in Figure 32.

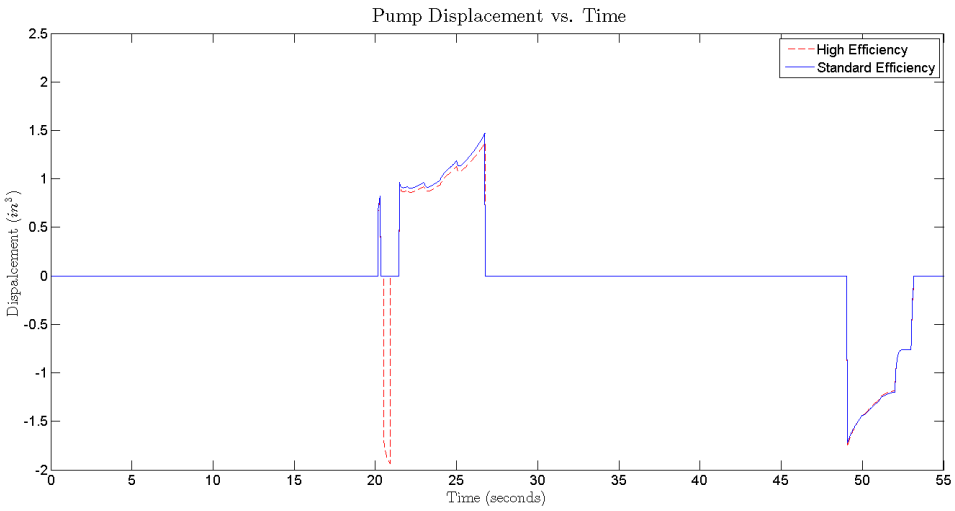

Figure 32. A Comparison of the pump displacement for the two evaluated pump efficiency maps during the first 55 seconds of the CBD drive cycle.

It was noticed that the difference in accumulator volume appeared to be the same before and after the deceleration. The displacement appeared to be the same for both

pumps during this period. During this period the efficiencies shown in Figure 33 are much closer than they were during the acceleration.

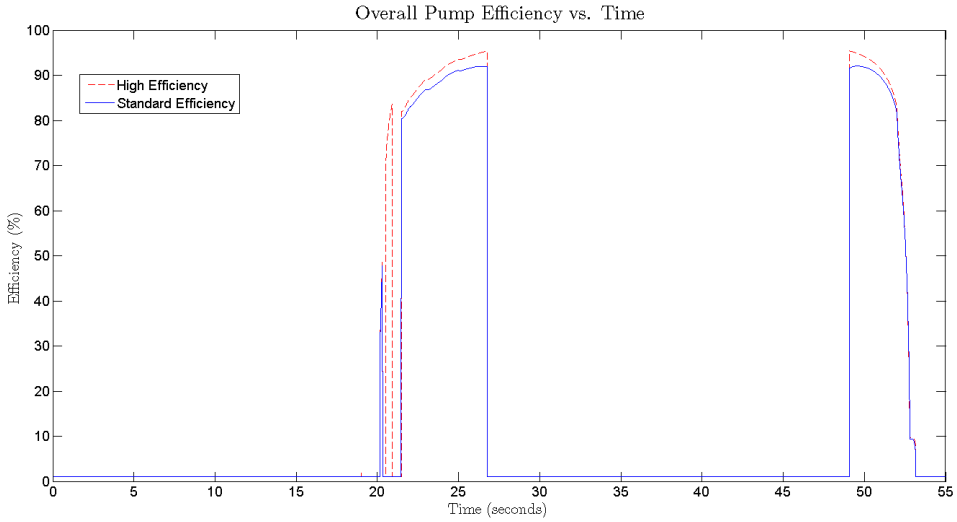

Figure 33. A Comparison of the pump efficiency for the two evaluated pump efficiency maps during the first 55 seconds of the CBD drive cycle.

Based on these observations, the efficiency of the pump has the potential to play a role in overall system performance. However, it does not have a large impact here because the overall displacement of the pump is much larger than what is being required of it. If the engine or pump were downsized, this may become more critical.

5.2.2 Accessory Loads

Despite the fact that the accessory loads were based on SAE specification J1343, there was still uncertainty associated with them. The model seemed to be very sensitive to this parameter as would be expected because many of these drive cycles have large periods of idling.

The base vehicle was assumed to have an air conditioner, but it is not necessarily a requirement for the vehicle. The average load specified in the SAE specification was 3

hp with a maximum load of 6 hp. To demonstrate this impact that this load has on the system the vehicle was simulated with a weight of 56,000 lbs, standard efficiency hybrid pump, and no load from the refuse body hydraulic circuit.

The results shown in Table 12 demonstrate how sensitive the model is to this parameter. Some of the results are quite significant. For instance the New York Garbage Truck Cycle only involves traveling 0.8 miles during a period of 760 seconds. The required energy to accelerate and propel the vehicle during this time was determined to be $9x10^{-4}$ hp-hr while the air conditioning system required 0.63 hp-hr during that same period. This cycle is an extreme case and is shown in Figure 34.

Table 12. The predicted fuel economy of hybrid vehicle with and without air conditioning.

	Fuel Economy With Air Conditioning (mpg)	Fuel Economy Without Air Conditioning (mpg)	Percent Improvement
NY Truck	5.20	8.03	54%
HUDDS	8.62	10.23	19%
NY Garbage Truck	3.66	8.12	122%
Orange Country Bus	7.39	9.74	32%
WVU City	6.47	9.93	54%
CBD	8.28	11.61	40%

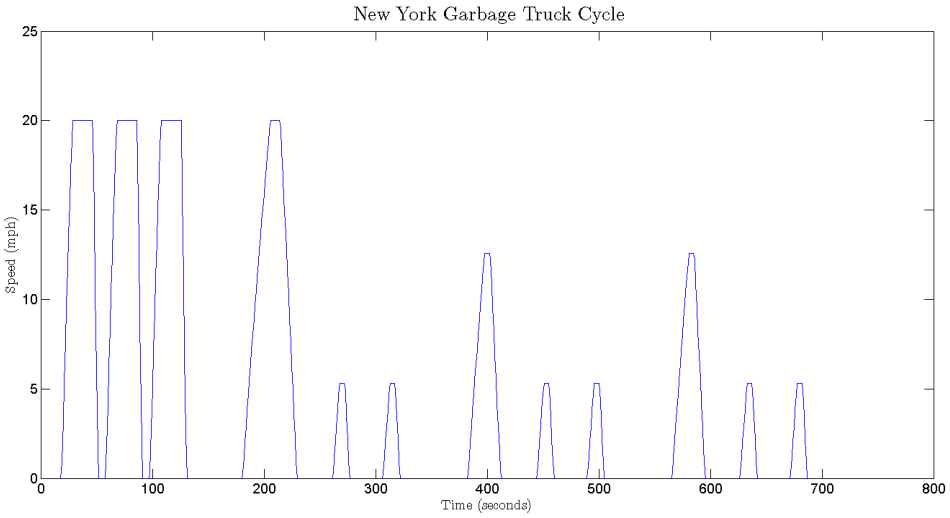

Figure 34. Speed profile of New York Garbage Truck drive cycle.

5.2.3 Transmission

The transmission used for this simulation was chosen based on model availability and commercial availability. A 5 or 6 speed torque converter type automatic transmission is a very popular choice for refuse trucks. However, a simulation model or data for this type of transmission was not available. Because of model availability, an automated manual transmission was chosen for this simulation. The specifications for gear ratios were taken from a commercially available transmission suitable for refuse trucks which had 10 forward speeds. This transmission was also used to model the conventional truck as well. This presents a problem because a different transmission will provide a different baseline level of performance.

To evaluate the difference that may be present with the automated manual transmission, a 6 speed manual transmission was evaluated. The specific transmission used for the specifications was a 5-speed Eaton Ultrashift HV and is made for medium duty trucks. Its gear ratios can be found in Table 13. It is not rated for refuse truck applications (Eaton Corporation, 2011e). It's also important to note that a 6th gear was

added to allow the vehicle to operate at high speeds. This gear was assumed to have the same ratio as the overdrive in the 10 speed transmission. Because of this change, this configuration does not represent a commercially available transmission.

Table 13. Gear ratios for alternate transmission used to evaluate effect of transmission used in model.

Gear	Ratio
1st	6.55
2nd	4.13
3rd	2.52
4th	1.59
5th	1.00
6th	0.73

The 6 speed transmission was implemented in the conventional vehicle to get an estimate of the impact it would have on the baseline truck. This simulation was run with a vehicle weight of 56,000 lbs, the standard efficiency pump, standard accessory loads, and no load from the refuse body hydraulic circuit. The resulting percent increase in fuel economy for the hybrid system with the 10-speed transmission is shown .

Table 14. Percent increase in fuel economy for implementation of hybrid system with 10 speed transmission over two conventional transmission configurations.

	Percent Increase over 6-Speed	Percent Increase Over 10-Speed
NY Truck	10%	5%
HUDDS	6%	3%
NY Garbage Truck	10%	5%
Orange Country Bus	18%	9%
WVU City	9%	3%
CBD	26%	15%

Even with these results, it is still unknown how much of an impact that the absence of a torque converter will have. Without exact performance data, it is hard to predict. However, Allison Transmission does specify the torque ratio at stall of the various torque converters offered with their transmissions. The 4000 HS transmission is offered with a range of torque converters. The torque ratio at stall varies from 1.58 for the TC-561 to 2.42 for the TC-521 (Allison Transmission, 2011). With these two stall torque ratios, the torque ratio and efficiency can be estimated over the range of speed ratios. The efficiency of the torque converter was estimated using Equation 43 from SAE specification J643 (Automatic Transmission Transaxle Committee, 2011).

$$\eta_{tc} = SR * TR \tag{43}$$

$$K = \frac{\omega_{input}}{\sqrt{\tau_{input}}} \tag{44}$$

The estimates for these curves can be seen in Figure 35. The maximum efficiency of both of these converters goes to 100% at a speed ratio of 1, but in reality this will never occur unless the torque converter "locks up". According to Eaton transmission literature, this does not occur until around 24 mph which roughly corresponds to when the hybrid system is disengaged. Without the corresponding capacity factor, which is defined in Equation 44, it is not possible to determine the operating point of the engine and torque converter.

If the torque converter is not locked up during the operating of the hybrid system, the efficiency of the torque converter could be drastically changed based on the operating

point. Based on this behavior of the torque converter, a potential for the hybrid system to improve the fuel economy of the vehicle does exist. Eaton also advertises in their literature for their automated manual transmissions that they can offer improvements in fuel economy of up to 23% (Eaton Corporation, 2011a).

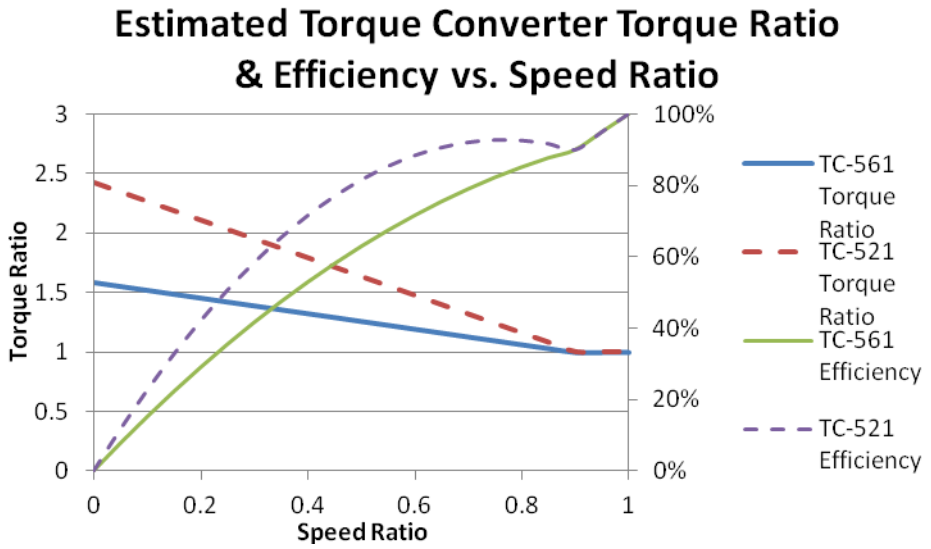

Figure 35. Estimated torque ratio and efficiency of two Allison torque converters available on 4000HS series transmission.

5.2.4 Accumulator Time Constant

The time constant of the accumulator was estimated to be about 10 seconds. Otis & Pourmovahed (1985) mention in their paper that this variable does not have a significant impact on predicting the behavior of the accumulator. However, this parameter was still investigated to insure that it did not significantly impact fuel economy because it was found analytically. Other methods exist for determining this value experimentally, but no data were available.

To determine this sensitivity, the time constant was assumed to be 0.1, 5, 10, 20, and infinity seconds. The value of 0.1 was used to approximate an isothermal accumulator, and the value of infinity was used to simulate an adiabatic system. These conditions were simulated with a vehicle weight of 56,000 lb, with the standard efficiency pump, standard accessory loads, no load from the refuse body hydraulic circuit, and the 10 speed transmission. The resulting fuel economies are shown in Table 15.

Table 15. Fuel economy of hybrid truck with varying time constant for the accumulator.

	Fuel Economy (mpg)				
	0.1 seconds	5 seconds	10 Seconds	20 seconds	Adiabatic
NY Truck	4.51	4.50	4.51	4.50	4.51
HUDDS	7.92	7.91	7.91	7.91	7.92
NY Garbage Truck	3.00	2.98	2.98	2.99	3.00
Orange Country Bus	6.66	6.60	6.61	6.62	6.65
WVU City	5.60	5.58	5.58	5.58	5.59
CBD	7.41	7.27	7.29	7.34	7.42

The effect of the time constant is not significant for the values of 5, 10, and 20 seconds. However, the adiabatic and isothermal assumptions do have a slight impact. It is believed that these two cases perform better because a lack of a change in pressure after a change in volume. Therefore, the controller is not trying to constantly hit a moving target that changes after the vehicle comes to a stop or reaches high speeds.

5.3 VEHICLE PERFORMANCE

Based on the analysis in the previous section, the set of values initially provided in Chapter 3 are the best possible set that accurately models a realistic vehicle with the available resources to the author. However, there are areas that offer potential for improvements. To estimate how the truck will perform, several drive cycles were used and more parameters were varied. The varied parameters include weight and the load of the refuse body hydraulic circuit. Then a new cycle was generated to estimate the complete duty cycle of the refuse truck to predict fuel economy.

5.3.1 Vehicle Weight & Hydraulic System Load

Unlike passenger cars, the weight of a heavy duty truck will vary considerable. The weight of a refuse truck will vary from trip to trip as well as during a trip while collecting garbage. To evaluate the impact of weight and estimate fuel consumption, the vehicle was simulated through several drive cycles at weights of 33,000 lbs, 40,000 lbs, 45,000 lbs, 50,000 lbs, and 56,000 lbs. The conventional truck weight was reduced by 1,350 lbs to account for the weight of the hybrid system.

The hydraulic system for the refuse body was also included in a portion of these simulations to assess the impact it has upon fuel economy when not being used. Because some refuse trucks power the pump through a PTO that is able to be disengaged while others have the pump mounted directly to the engine, both cases are valid. The load of the hydraulic circuit functioning was not evaluated because it was assumed that it would only be operated while the vehicle was at rest when the hybrid system cannot function.

The results of the set of simulations for the Central Business District Cycle (CBD) are shown in Figure 36, and a plot of the drive cycle is shown in Figure 37. The results show that both the fuel economy of the vehicle and the performance of the hybrid system are dependent upon weight. As weight increases the fuel economy decreases because of

an increase in rolling resistance of the vehicle and the larger amount energy that is dissipated through braking. Because the hybrid is able to recapture a significant portion of the energy that is lost through braking, its performance increases with the addition of weight. The cause of the knee in the curve for the conventional truck with the hydraulic system load is unknown.

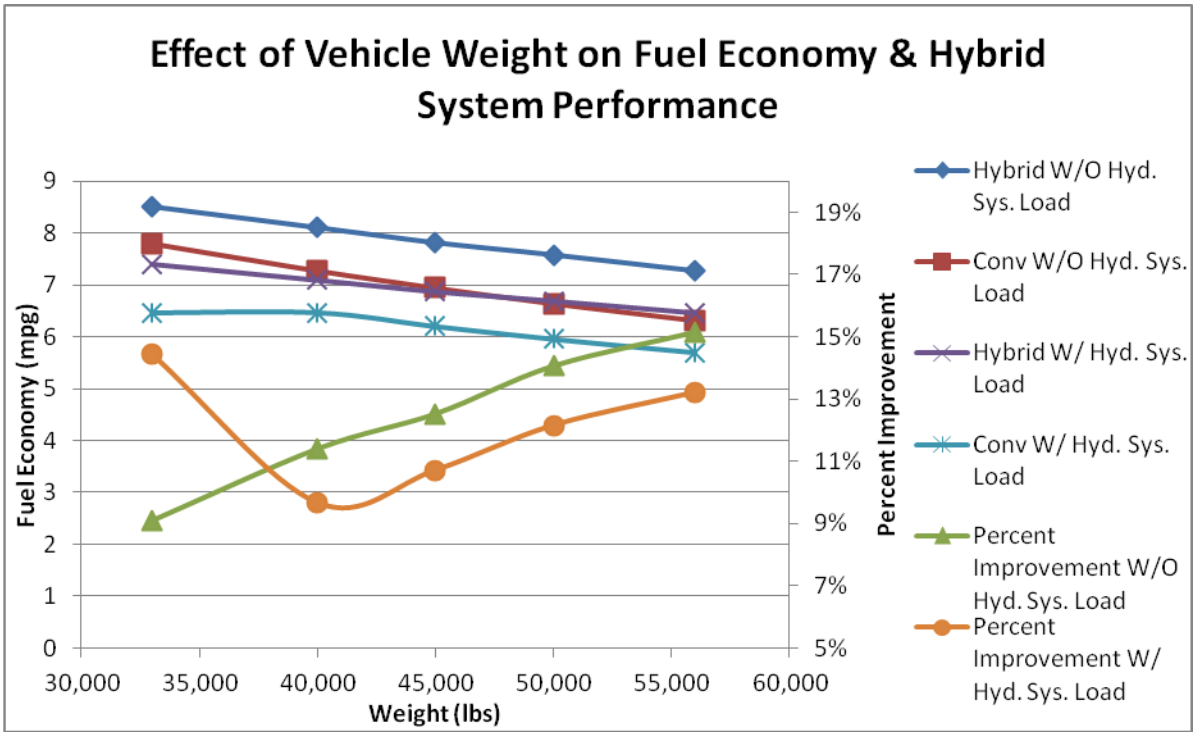

Figure 36. Estimated fuel economy and percent improvement of refuse truck as weight varies for CBD drive cycle.

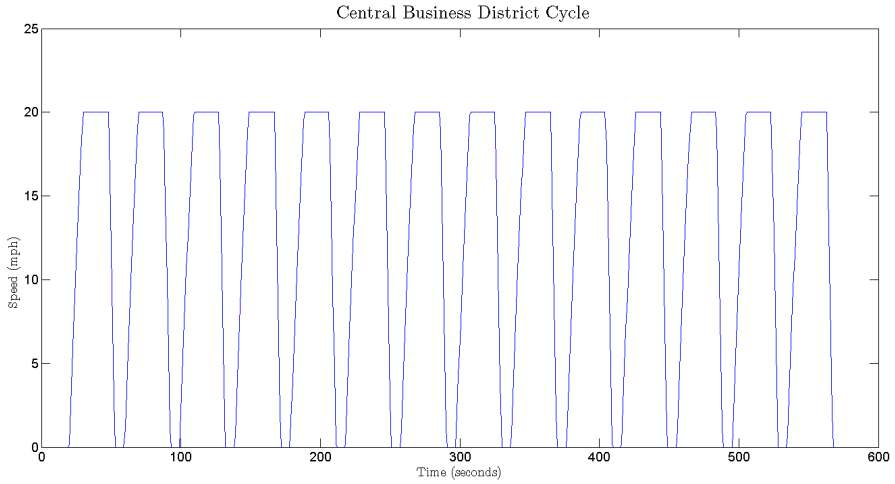

Figure 37. Speed vs. time profile of Central Business District Cycle.

While it is important to show how well the hybrid system can perform under desirable conditions, it is also important to show how it performs under other conditions that are not ideal. Figure 38 shows the estimated fuel economy and hybrid system performance for the Heavy Duty Urban Dynamometer Driving Schedule (HUDDS). This cycle has speeds as high as 58 mph with some stop and go driving as well. This cycle is shown in Figure 39. The hybrid system does not perform as well on this cycle because the cycle has fewer stops. It also has longer periods of time operating at speeds above that which the hybrid system can operate. This type of operation may not be the predominant type of operation that a refuse sees, but it may represent a portion of the time spent traveling to and from the landfill.

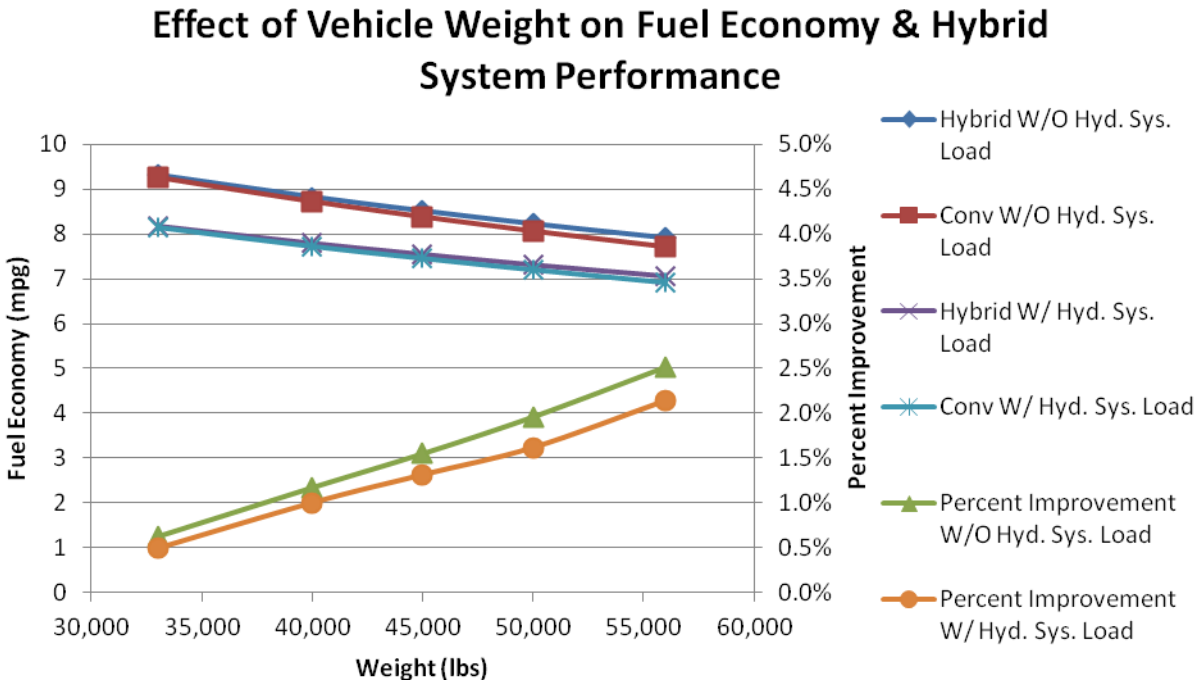

Figure 38. Estimated fuel economy and percent improvement of refuse truck as weight varies for HUDDS drive cycle.

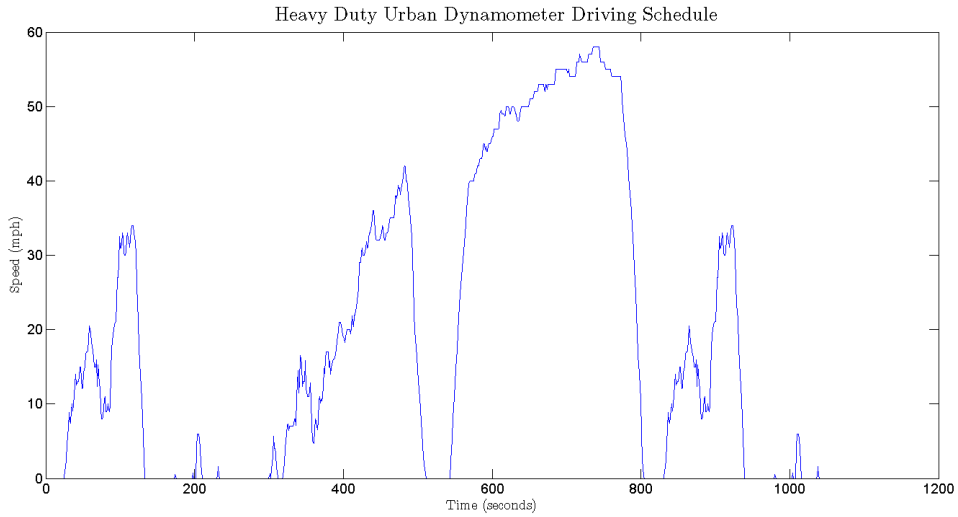

Figure 39. Speed vs. time profile of Heavy Duty Urban Dynamometer Driving Schedule.

5.3.2 Final Estimated Fuel Economy

The final fuel economy for the vehicle that is used for the analysis in the next chapter was estimated using a combination of drive cycles. The created drive cycle consisted of a combination of the HUDDS cycle and the CBD cycle and is shown in Figure 40. The creation of this cycle was based off of a cycle that was generated from many days of refuse truck data collect in the City of New York. However, a copy of that cycle was not available. The New York Garbage Truck Cycle was not used because it represents some of the most severe conditions and very low speeds (Ivanič, 2007). While the CBD cycle may not necessarily represent an actual refuse truck cycle, it is most likely a close approximation.

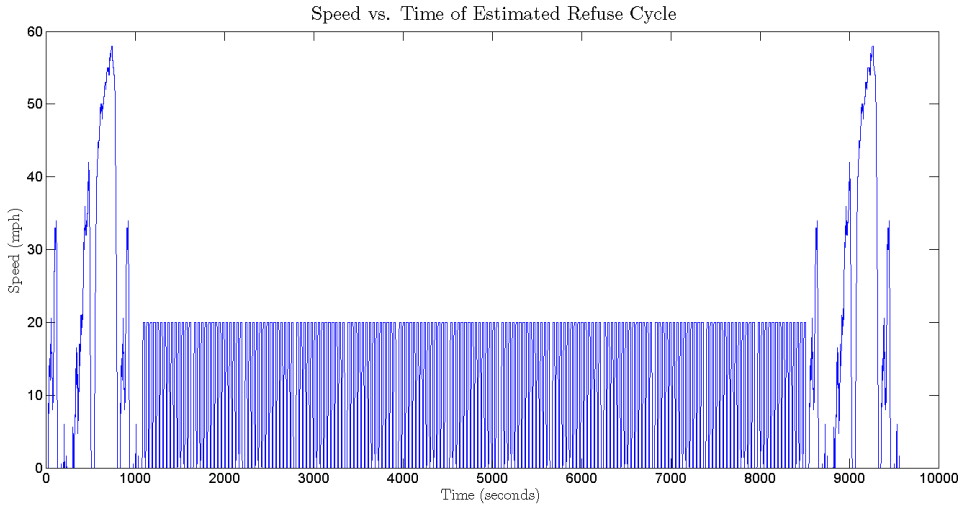

Figure 40. Speed profile of hypothetical drive cycle that was generated from a combination of the HUDDS and CBD cycles.

This new cycle also included the change in weight of the vehicle as refuse is collected. Two approaches were taken for this change in weight. The first was to assume that the truck would be limited by weight at 56,000 lbs. The second approach was to

assume that the truck would "cube out" by filling the entire volume of the refuse body before reaching its maximum weight. The final weight of the system was then assumed to be 50,000 lbs. The addition of the weight occurred at discrete instants in time. This occurred at the end of each repetition of the CBD cycle. The addition of weight as a function of time for the cubed out cycle can be seen in Figure 41.

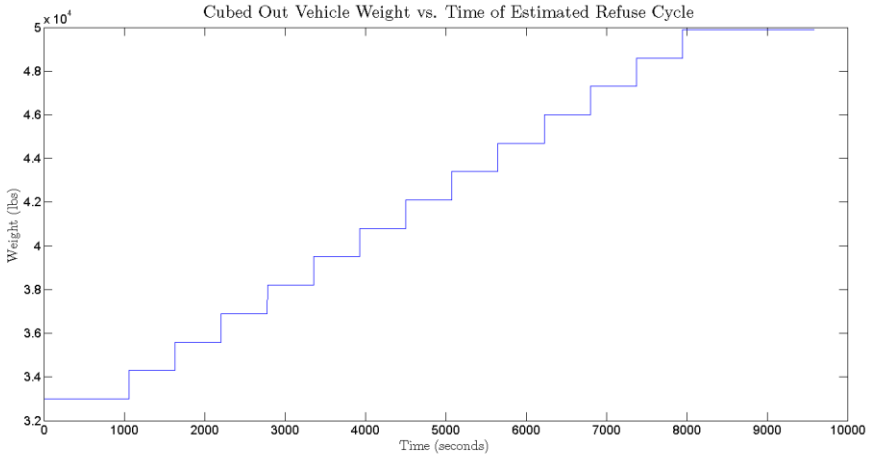

Figure 41. Addition of weight as a function of time for hypothetical drive cycle.

The final estimation of fuel economy is shown as the average of the "cubed out" and "weighed out" conditions in Table 16. While these values may represent a prediction for fuel economy much higher than that of actual refuse truck data, they still are useful data points because their difference reflects the fuel savings of the hybrid system. These values would be much lower if the function of the refuse body hydraulic circuit were included. The power of the system at 2500 psi and 42 gpm is 61.3 hp. This coupled with the sensitivity of fuel economy to accessory loads demonstrated in a previous section should drastically reduce these values.

Table 16. Estimated fuel economy for various vehicle configurations for hypothetical drive cycle.

	Conv. Without Hydraulic System Load	Conv. With Hydraulic System Load	Hybrid Without Hydraulic System Load	Hybrid With Hydraulic System Load
Cube Out	7.98	7.05	8.50	7.44
Weight Out	7.91	7.00	8.42	7.38
Average	7.95	7.02	8.46	7.41

Chapter 6: Hybrid System Cost Analysis

While it is very important that the system reduces fuel consumption, the resulting cost savings are also very important. If the system does not pay for itself or come close to that point, it will be very difficult to justify its adoption. A survey conducted by Beverage World showed that many beverage distributors adopt "green fleet" practices because of corporate philosophy rather than to save money (Cioletti, McCall, & Saltsgiver, 2011). These results are presented in Figure 42. Even though the primary reason for adoption may not be cost, it is still important because opting for a hybrid fleet must be affordable.

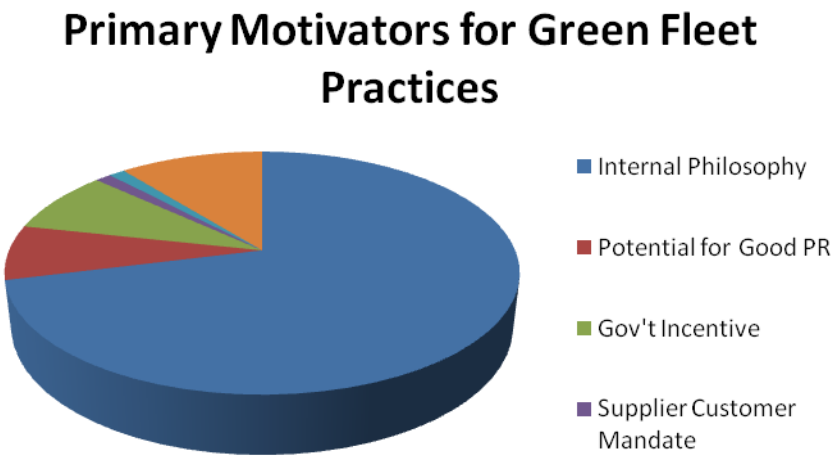

Figure 42. Reasons for adopting green fleet practice for beverage distributors (Cioletti et al., 2011).

6.1 Estimated Hybrid System Maintenance Costs

Just like the oil in a car, the oil in a hydraulic system must be periodically changed. In addition to this maintenance other components must be serviced and periodically checked. Items that wear and need replacement on hydraulic hybrids are the

transfer case oil, hydraulic fluid, breather, system oil filter, secondary oil filter, accumulator bladder, and accumulator gas charge.

It should be noted that this chapter is an updated version of Appendix B presented in "Hybrid Distribution Trucks: Costs and Benefits". The updated version more closely represents the actual system now that better data is available (G. Anderson & Harrison, 2011).

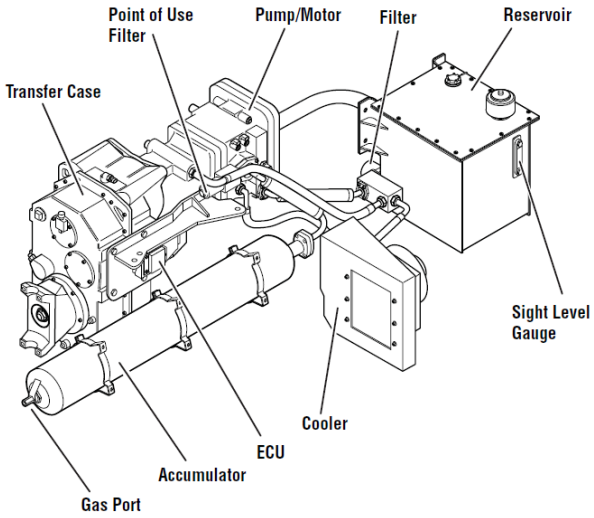

Figure 43. Line drawing of Eaton Hydraulic Launch Assist sytem (Eaton Corporation, 2011d).

The hydraulic fluid in a system serves several purposes. The first purpose is to transmit power. The other two functions are to help cool and lubricate the system (Esposito, 2003). As the fluid ages some of properties change making it less suitable for the system, and it must be changed (Eaton Corporation, 2006). The fluid capacity of the hydraulic system was specified by the service manual to 21 gallons. The price for a gallon of hydraulic fluid was estimated to be $8.00/gallon. This was based on prices obtained from O'Reilly Auto Parts for a 5 gal bucket of AW46 hydraulic fluid (O'reilly

Auto Parts, 2010). The service manual specifies a specific Eaton fluid for the system, but no information could be found. So it was assumed that the price of a general fluid would have a comparable cost to the Eaton fluid. It was estimated that it would take 3 hours to change the oil in the system at a labor cost of $50/hour. With these assumptions the cost of a fluid change would be $378.

The breather on the hydraulic reservoir typically has two functions. The first is to allow air to enter and exit the reservoir as the fluid level within the reservoir changes. Its other function is to filter the air as it enters the reservoir to minimize oil contamination. Components in hydraulic systems have very tight clearances. Therefore small pieces of dirt and other material can significantly degrade the performance of the system if allowed into the oil. Over time the filter in the breather will become clogged and need replacement. The breather was estimated to cost $15 based on the author's personal experience as a hydraulic systems engineer. The labor was estimated to be ½ hour. Therefore a breather change should be about $40.

The filter for a hydraulic system is very similar to an engine oil filter. However, they can be much larger when higher flows are required by the system. Both filters for this system use a filter design where the element rather than the assembly that includes the metal "can" is changed like on an engine. Figure 44 shows an exploded view of this design. The advantage to this design is that there is less trash generated and the reduced material requirements reduce cost. The two filters for the system were estimated to have a combined cost of $50. It was also assumed that this maintenance would be conducted in conjunction with a system oil change. So no labor was included for this item.

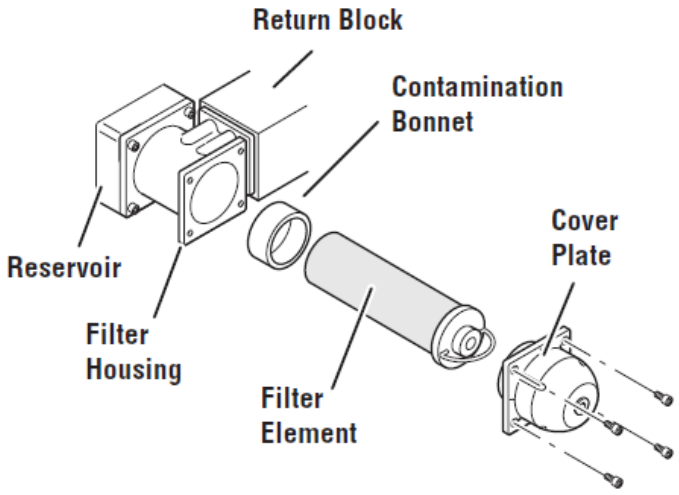

Figure 44. Exploded view of main system oil filter (Eaton Corporation, 2011d).

The accumulator is the energy storage device for the hydraulic hybrid system. It is able to store energy through the compression of nitrogen gas stored in the bladder (Esposito, 2003). Over time this bladder can become worn from the compression and expansion it experiences as oil enters and exits the accumulator. Constant exposure to oil can also degrade the rubber over time. The gas charge contained in the bladder can also leak through the rubber over time much like helium in a latex balloon. Periodically the charge in the accumulator must be checked and refilled if found to be low. This aspect of the maintenance was not considered because it was unknown how often this might occur, is mostly likely a small cost, and the charge would be refilled every 2 years when the bladder is changed.

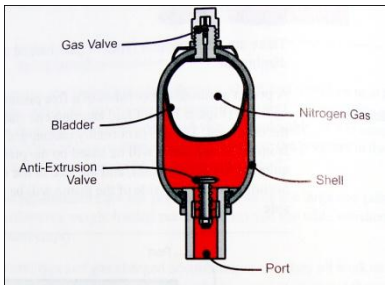

Figure 45. Cross sectional view of bladder type accumulator (Eaton Corporation, 2006).

The service manual specifies that the accumulator bladder must be changed every 2 years. The exact cost of the replacement parts was unknown, and costs of similar parts were not available. To estimate this cost replacement bladders for smaller accumulators were priced at McMaster Karr. A curve was then fit to the costs to extrapolate what a 15 gallon accumulator bladder would cost. The resulting fit can be seen in Figure 46. The estimated cost of the bladder was $725. The labor was assumed to be 8 hours because the accumulator must be removed from the vehicle and be completely disassembled. With these assumptions the total cost is estimated to be $1125.

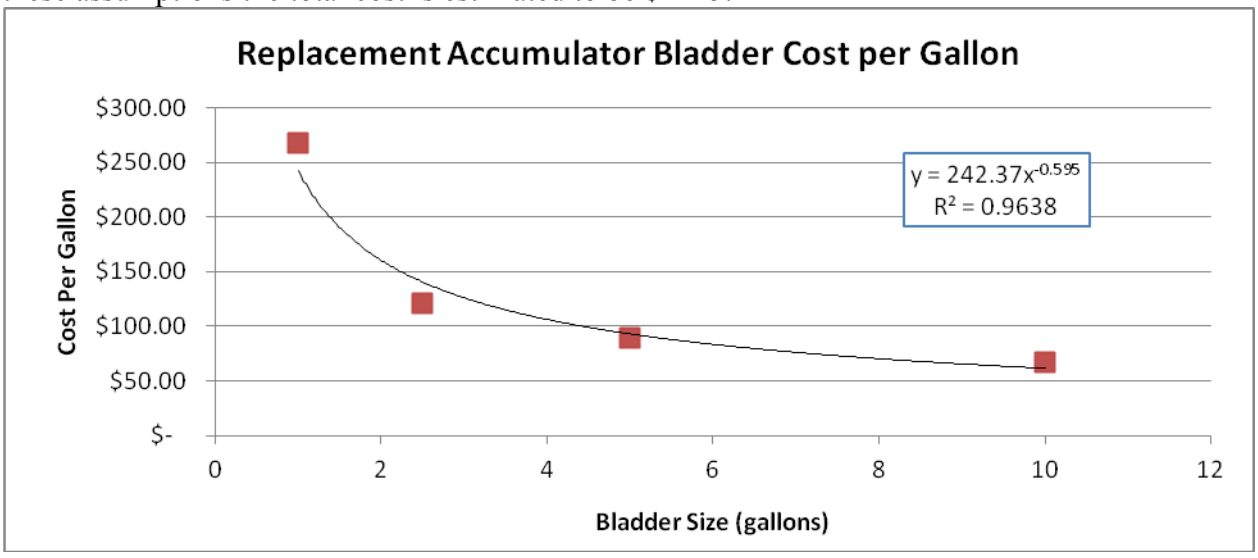

Figure 46. Replacement accumulator bladder cost per gallon as a function of bladder size (McMaster-Carr, 2011).

The transfer case is not a component in the hydraulic system, but is required to couple the hydraulic system to the drivetrain. The service manual specifies that its fluid must be changed every 5 years. The capacity of the transfer case is 1.9 gallons, and the fluid is a 75W-90 gear synthetic oil (Eaton Corporation, 2011d). The estimated price of this oil was $25/gal. This was derived from oils that were available at O'Reilly Auto Parts which ranged from $15 to $32 per gallon (O'reilly Auto Parts, 2010). If this task takes 2 hours to complete, the total cost will be $147.50.

Table 17. Hydraulic hybrid maintenance items and estimated costs for each item including labor.

Maintenance Item	Frequency (months)	Cost
Fluid change	12	$ 378.00
Filter change	12	$ 60.00
Transfer case oil change	60	$ 147.50
Breather replacement	12	$ 40.00
Accumulator bladder replacement	24	$ 1,125.00

6.2 Economic Analysis

The cost estimate included the initial hybrid system cost, interest, depreciation, brake repair savings, and maintenance costs. The hybrid system was evaluated at 3 different costs of $20,000, $25,000, and $30,000. The interest was assumed to be 4% simple interest, and the depreciation was estimated using the fixed declining balance method built into Excel. The final value of the system was assumed to be $5,000. The total period of ownership was assumed to be 10 years.

The advertised brake savings for the adoption of the hydraulic hybrid system has ranged from 2X to 4X the current brake life. To confirm this fact, the energy dissipated by the brakes was monitored in the simulation. The brakes on the conventional truck

were found to dissipate 2.3 times more energy than the hybrid. Therefore the brake life was assumed to only double with the hybrid system. The conventional truck was assumed to have its brakes serviced every 4 months.

The fuel price was assumed to be $4.00/gallon. The current national average price of diesel at the pump for the week of October 31, 2011 is $3.892/gallon (U.S. Department of Energy, 2011).

The estimated cost of ownership is presented for two cases that exclude and include the load from the refuse body hydraulic circuit. These two cases are presented in Figure 47 and Figure 48. Neither case appears to pay for itself. However, this may be due to the fact that the conventional truck may be more efficient than the truck that is actually being replaced. The rough shape of the lines is caused by the maintenance items occurring at the specified intervals.

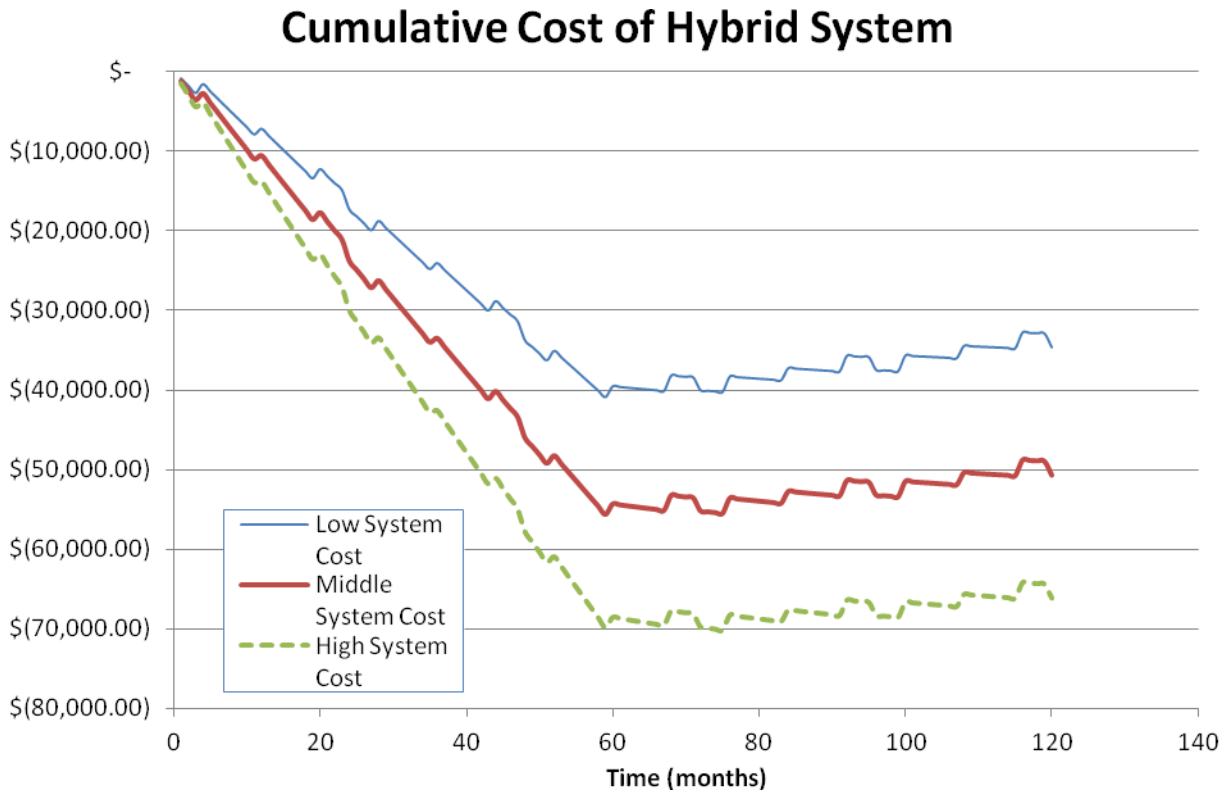

Figure 47. Estimated cost of hybrid system ownership for a hydraulic hybrid refuse truck without hydraulic system load.

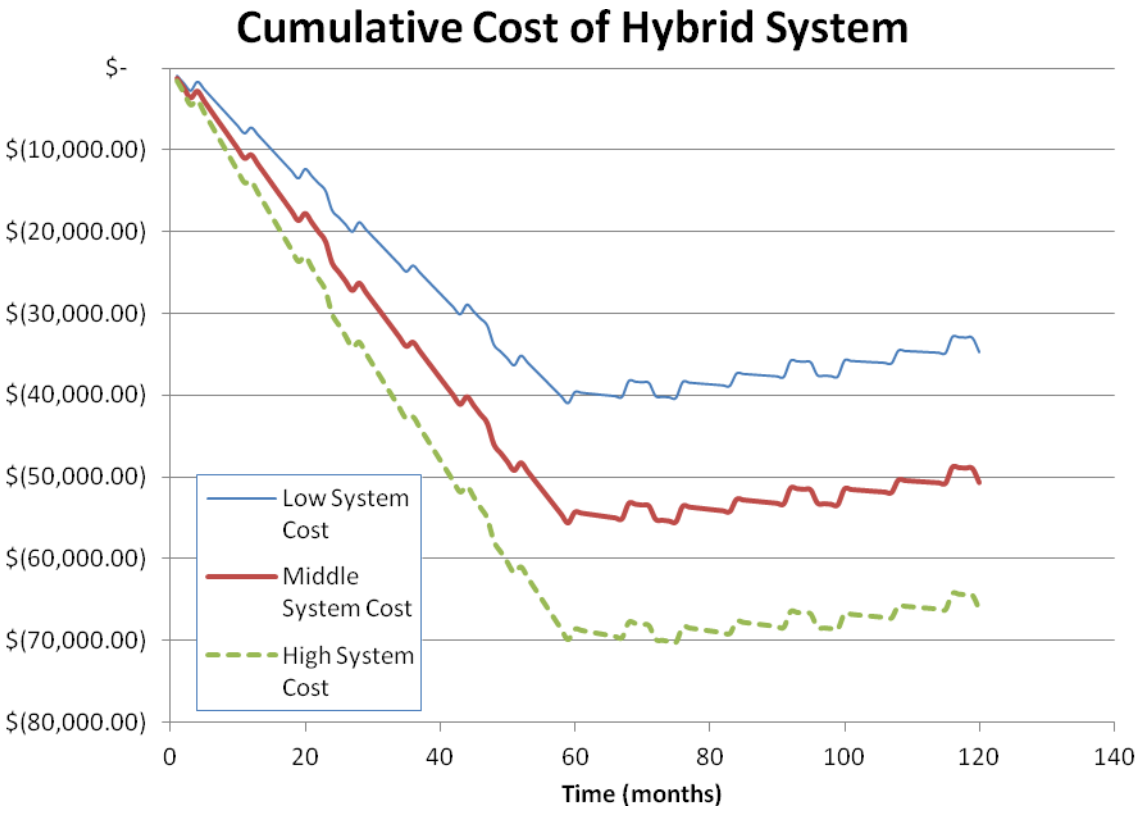

Figure 48. Estimated cost of ownership for a hybrid system that includes load from the hydraulic system.

Chapter 7: Conclusions and Future Work

Based on the results of this study, a hydraulic hybrid system does not make financial sense. However, there are some discrepancies that need to be further investigated before making a definitive decision.

It has been shown that the configuration of the transmission is very important to the overall efficiency of the vehicle. While the hydraulic system is able to deliver improvement in fuel economy through the capture of energy that would normally be lost as heat through braking, it is also able to increase the efficiency of the drivetrain by allowing for optimal loading of the engine and other components. With the automatic transmission this is even more important because of the wide range of the efficiency of the torque converter. This aspect of its behavior warrants further investigation.

Despite the uncertainty about the resulting costs, there may be conclusions that can still be drawn. It may actually make more sense to purchase a refuse truck with an automated manual rather than a hydraulic hybrid system at the current time. However, there may be performance differences between the two systems that must be considered. Allison Transmission advertises in their literature that their torque converter type transmissions offer improved acceleration over an automated manual transmission (Allison Transmission, 2011). This decision may be dictated on the performance requirements of the vehicle. If the automatic transmission is more desirable, then the hydraulic hybrid may offer a larger benefit.

The other interesting question that these results pose is how the performance of hybrid systems will be impacted as other portions of the drivetrain are improved. The EPA and NHTSA have adopted new regulations that will regulate heavy-duty trucks on a basis of g CO_2/ton-mile and gal/1000 ton-mile. These regulations were designed to

increase the efficiencies of these vehicles (United States Environmental Protection Agency, 2011). As new technologies are adopted, the losses that hybrids reduce may overlap. This in turn will reduce the benefit of the hybrid system. A study conducted by the Northeast States Center for a Clean Air Future, International Council on Clean Transportation, Southwest Research Institute, and TIAX on implementing several technologies for long haul trucks demonstrated this concept by showing that the individual increases in efficiency for each technology do not simply add when using both are used in conjunction (Cooper, Kamakaté, Reinhart, & Wilson, 2009).

Even though these results do not show a benefit for a hydraulic hybrid system, it does not prove that it is not a viable option. It does show that the vehicle used as the baseline may have a large impact on its incremental improvement. It also shows that the driving conditions that the vehicle is exposed to are critical to its performance. As this technology is adopted and further refined, these behaviors will become more apparent.

7.1 Future Work

Based on the available information used for this study and the data gathered from the various simulations, several logical steps present themselves for potential future work.

1. The construction of an automatic transmission model would greatly improve the prediction of this model. This model would help to confirm the advertised incremental improvement of the system and could easily be implemented in the programs written for the control policy formulation and vehicle simulation. With this alternate vehicle configuration, it would help to better understand how the hybrid system behaves in order to increase vehicle efficiency with an automatic vs. an automated manual transmission.

2. A brake wear model would be another beneficial piece of work. The hydraulic hybrid system has shown a wide range in the reductions of brake wear. A brake wear model would help to better understand what factors cause these variations. In addition to the wear model a more in depth review of the maintenance costs should be performed.
3. Improved models for the accessory loads could be beneficial. The method used in this study was an approximation of the actual loads. Improved models could add some validity to results based on the sensitivity that the model has shown to these loads.

Appendix A: Drive Cycles

The following drive cycles were used for control policy development, vehicle simulation, or both.

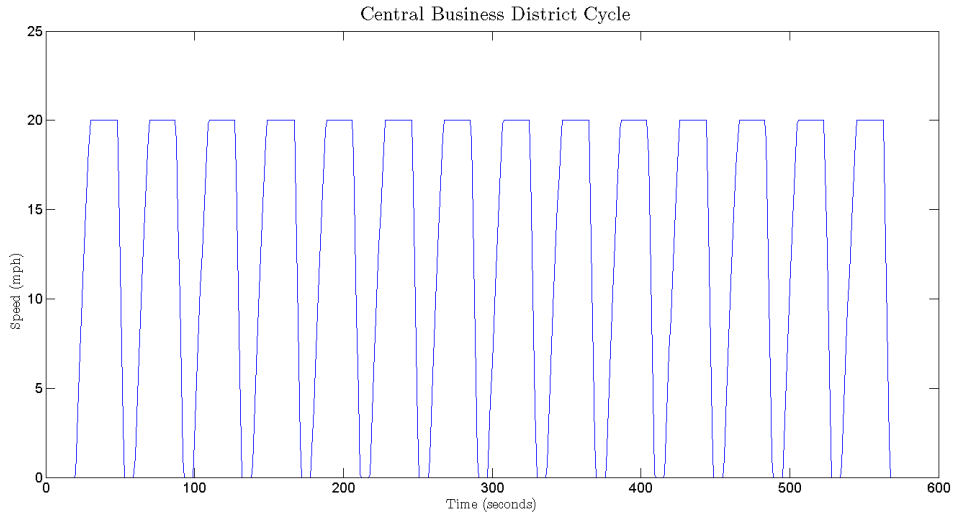

Figure 49. Speed profile of Central Business District drive cycle.

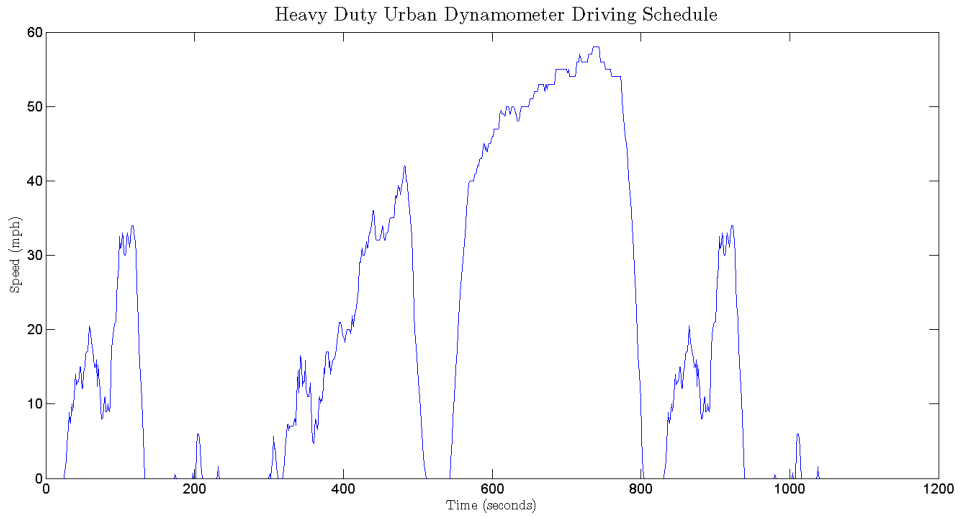

Figure 50. Speed profile of Heavy Duty Urban Dynamometer Driving Schedule.

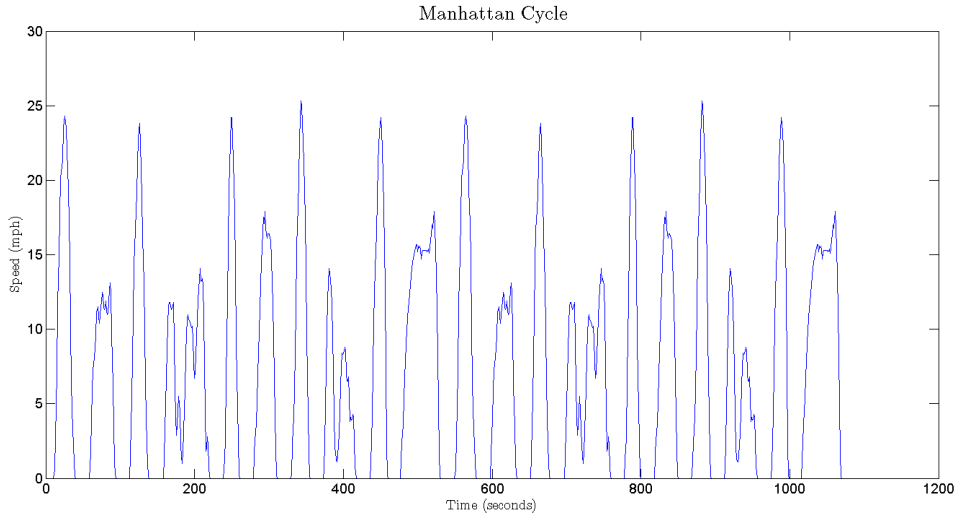

Figure 51. Speed profile of Manhattan drive cycle.

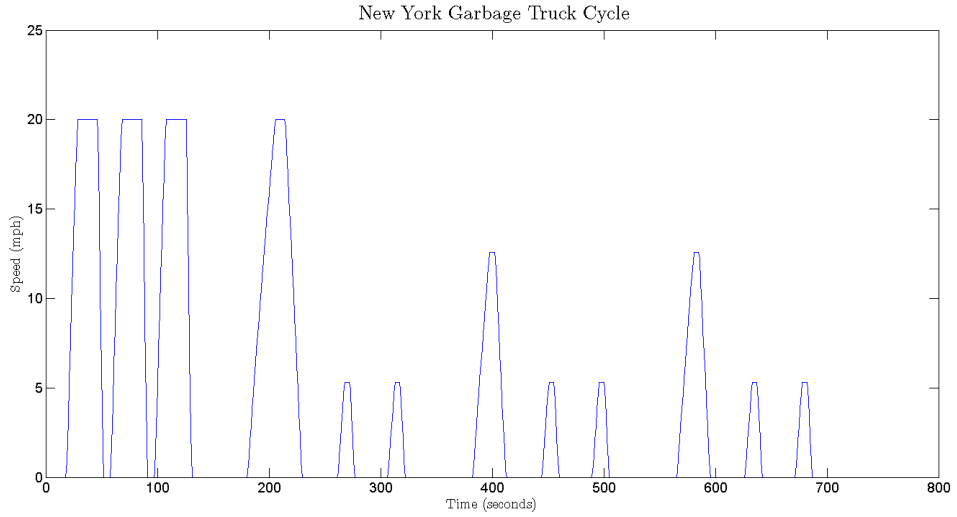

Figure 52. Speed profile of New York Garbage Truck drive cycle.

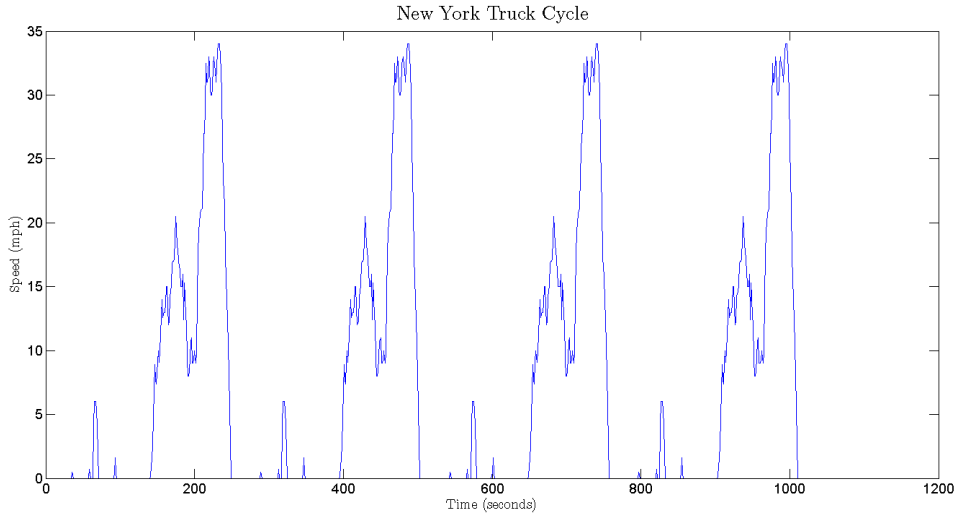

Figure 53. Speed profile of New York Truck drive cycle.

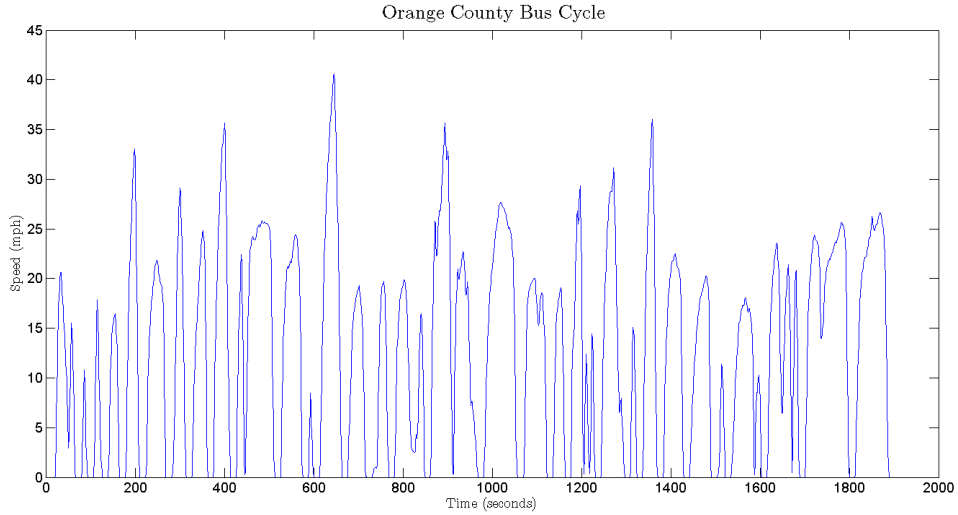

Figure 54. Speed profile of Orange County Bus drive cycle.

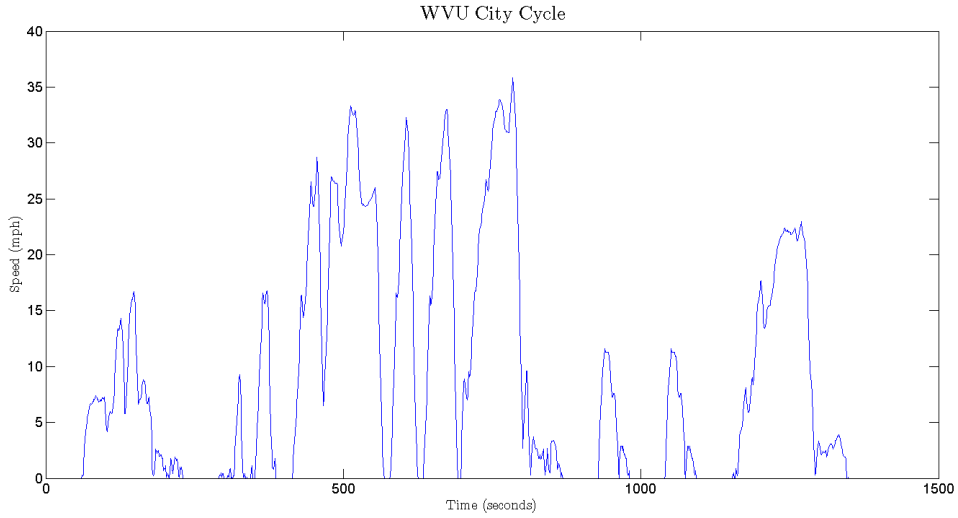

Figure 55. Speed profile of West Virginia University City drive cycle.

Bibliography

(Canada), T. D. C., Drozdz, P., & Technologies, V. (2005). *Hybrid refuse truck feasibility study*. Transportation Development Centre.

Abuhaiba, M., & Olson, W. W. (2010). Geometric and Kinematic Modeling of a Variable Displacement Hydraulic Bent-Axis Piston Pump. *Journal of Computational and Nonlinear Dynamics*, *5*(4), 041010 (12 pp).

Advanced Technology Division. (2004). *Progress Report on Clean and Efficient Automotive Technologies Under Development at EPA: Interim Technical Report*. United States Environmental Protection Agency. Retrieved from http://www.epa.gov/otaq/technology.htm

Akers, A., Gassman, M., & Smith, R. (2006). *Hydraulic Power System Analysis* (1st ed.). Boca Raton, Florida: CRC Press.

Allison Transmission. (2011). Rugged Duty Series. Retrieved from http://www.allisontransmission.com/servlet/DownloadFile?Dir=publications/pubs&FileToGet=SA3743EN.pdf

Anderson, G., & Harrison, R. (2011). *Hybrid Distribution Trucks: Costs and Benefits* (No. SWUTC/11/476660-00080-1). Austin, Texas: Center for Transportation Research.

Automatic Transmission Transaxle Committee. (2011). *Hydrodynamic Drive Test Code* (SAE Specification No. J643). Warrendale, PA: SAE International.

Barry, K. (2008, October 28). UPS to Roll Out Hydraulic Hybrids. Conde Nast Digital. Retrieved from http://www.wired.com/autopia/2008/10/ups-hydraulic-h/

Berendsen Fluid Power, Inc. (1990). *Fluid Power Designers' Lightning Reference Handbook* (8th ed.). Tulsa, Oklahoma: Berendsen Fluid Power, Inc.

Bosch Rexroth AG. (2011, July 8). Bosch Rexroth Industrial Hydraulics. Retrieved August 5, 2001, from http://www.boschrexroth.com/industrial-hydraulics-catalog/Vornavigation/VorNavi.cfm?PageID=p77749&Language=en

Butler, K., Hammerschmidt, S., Steiner, F., & Zhang, M. (2009). *Reinventing the Texas Triangle: Solutions for Growing Challenges*. Austin, Texas: The University of Texas at Austin Center for Sustainable Development. Retrieved from http://soa.utexas.edu/files/csd/ReinventingTexasTriangle.pdf

Cengel, Y. (2001). *Selected Material from Fundamentals of Thermal-Fluid Sciences*. New York, NY: McGraw-Hill Higher Education.

Chan-Chiao Lin, Huei Peng, & Grizzle, J. W. (2004). A stochastic control strategy for hybrid electric vehicles. *American Control Conference, 2004. Proceedings of the 2004* (Vol. 5, pp. 4710-4715). Presented at the American Control Conference, 2004. Proceedings of the 2004, IEEE.

Chan-Chiao Lin, Huei Peng, Grizzle, J. W., & Jun-Mo Kang. (2003). Power management strategy for a parallel hybrid electric truck. *IEEE Transactions on Control Systems Technology*, *11*(6), 839- 849. doi:10.1109/TCST.2003.815606

Chandler, K., Norton, B. P., & Clark, N. (2001). Waste Management's LNG Truck Fleet: Final Results. *DOE Report, January*.

Cioletti, J., McCall, M., & Saltsgiver, S. (2011, February 24). *Green Fleets: The Road Ahead*. Beverage World Webinar. Retrieved from http://event.on24.com/r.htm?e=278521&s=1&k=8904CD52A1210A740E3E85004CED53C4

City of Washington, PA. (2011). City of Washington. Pinnacle Computing. Retrieved from http://washingtonpa.us/index.html

Cooper, C., Kamakaté, F., Reinhart, T., & Wilson, R. (2009). Reducing Heavy-Duty Long Haul Combination Truck Fuel Consumption and CO2 Emissions. *NESCCAF*.

Desai, C., & Williamson, S. S. (2009). Comparative study of hybrid electric vehicle control strategies for improved drivetrain efficiency analysis. *2009 IEEE Electrical Power & Energy Conference (EPEC)* (pp. 1-6). Presented at the 2009 IEEE Electrical Power & Energy Conference (EPEC), IEEE. doi:10.1109/EPEC.2009.5420888

Dunn, H., & Wojciechowski, P. (1972). High Pressure Hydraulic Hybrid with Regenerative Braking. *Proceedings of 7th Intersociety Energy Conversion Engineering Conference, San Diego* (p. 989).

Eaton Corporation. (2005). Eaton-Vickers: Accumulators. Retrieved from http://hydraulics.eaton.com/products/pdfs/V-FIFI-MC003-E.pdf

Eaton Corporation. (2006). *Eaton Mobile Hydraulics Manual*. Eden Prairie, Minnesota: Eaton Corporation.

Eaton Corporation. (2009, April). Success Story: City of Denver Colorado. Retrieved from

http://www.eaton.com/ecm/groups/public/@pub/@eaton/@corp/documents/content/pct_221556.pdf

Eaton Corporation. (2011a). Vocational Series. Retrieved October 31, 2011, a from http://www.roadranger.com/Roadranger/productssolutions/transmissions/UltraShiftPLUS/VocationalApps/index.htm

Eaton Corporation. (2011b). D170 Series. Retrieved August 13, 2011, b from http://www.roadranger.com/Roadranger/productssolutions/drive,steer,traileraxles/d170heavydutytandemaxles/index.htm

Eaton Corporation. (2011c). UltraShift LST. Retrieved August 10, 2011, c from http://www.roadranger.com/Roadranger/productssolutions/transmissions/UltraShiftLST/index.htm

Eaton Corporation. (2011d, November). Service Manual: Eaton Hydraulic Launch Assist (HLA). Eaton Corporation. Retrieved from www.eaton.com/ecm/idcplg?IdcService=GET_FILE&dID=386313

Eaton Corporation. (2011e). Transmissions. Retrieved October 17, 2011, e from http://www.roadranger.com/Roadranger/productssolutions/transmissions/index.htm

Ehsani, M., Gao, Y., & Emadi, A. (2009). *Modern Electric, Hybrid Electric, and Fuel Cell Vehicles: Fundamentals, Theory, and Design, Second Edition* (2nd ed.). Boca Raton, Florida: CRC Press.

Esposito, A. (2003). *Fluid power with applications* (6th ed.). Columbus, OH: Prentice Hall.

Filipi, Z., Louca, L., Daran, B., Lin, C. C., Yildir, U., Wu, B., Kokkolaras, M., et al. (2004). Combined optimization of design and power management of the hydraulic hybrid propulsion system for the 6X6 medium truck. *International Journal of Heavy Vehicle Systems*, *11*(3), 372–402.

Geartek. (2008). Geartek.net. Retrieved October 19, 2011, from http://www.geartek.net/

Gray Jr, C. (2006, October 17). *Hydraulic Hybrids: EPA Hybrid Truck Initiative*. Houston, Texas.

Ivanič, Ž. (2007). Data Collection and Development of New York City Refuse Truck Duty Cycle. *SAE Technical Paper*, 01–4118.

Karnopp, D. C., Margolis, D. L., & Rosenberg, R. C. (2006). *System Dynamics: Modeling and Simulation of Mechatronic Systems* (4th ed.). Hoboken, New Jersey: Wiley.

Kim, Y. J., & Filipi, Z. (2007). Simulation study of a series hydraulic hybrid propulsion system for a light truck. *SAE paper*, 01–4151.

Labrie. (2010). Leach: 2R-III Spec Sheet. Retrieved from http://www.labriegroup.com/en/

Lammert, M., & (US), N. R. E. L. (2009). *Twelve-month evaluation of ups diesel hybrid electric delivery vans*. National Renewable Energy Laboratory.

Manring, N. (2005). *Hydraulic Control Systems* (1st ed.). Hoboken, New Jersey: Wiley.

Matthews, R. D., Ates, M., Dardalis, D., Kim, K. J., Vaughn, J., Hao, L., Anderson, G., et al. (2011). *Texas Motor Vehicle Operating Costs; Final Report* (Texas Department of Transportation (TxDOT) Technical Report No. 0-5974-2). Center for Transportation Research, Bureau of Engineering Research, The University of Texas at Austin.

Matthews, Ronald Douglas. (2010). *Internal Combustion Engines and Automotive Engineering*. Austin, Texas.

McMaster-Carr. (2011). McMaster-Carr. Retrieved May 20, 2011, from http://www.mcmaster.com/#hydraulic-accumulators/=ce3i4t

Merritt, H. E. (1967). *Hydraulic Control Systems* (1st ed.). New York, NY: Wiley.

Michelin. (2011). Michelin Americas Truck Tires XDY® 3 Page. Retrieved October 17, 2011, from http://www.michelintruck.com/michelintruck/tireSelector.do

Munson, B. R., Young, D. F., & Okiishi, T. H. (2001). *Fundamentals of Fluid Mechanics* (4th ed.). Hoboken, New Jersey: Wiley.

National Institute of Standards and Technology. (2011). NIST Chemistry WebBook. Retrieved October 22, 2011, from http://webbook.nist.gov/chemistry/

National Renewable Energy Laboratory. (2011, March). Project Startup: Evaluating Coca-Cola's Class 8 Hybrid-Electric Delivery Trucks. Retrieved from http://www.nrel.gov/docs/fy11osti/49621.pdf

O'reilly Auto Parts. (2010). O'Reilly Auto Parts. Retrieved from http://www.oreillyauto.com/site/c/search/Diesel+Exhaust+Fluid/N2204/C0014.oap

Otis, D., & Pourmovahed, A. (1985). Algorithm for computing nonflow gas processes in gas springs and hydropneumatic accumulators. *Journal of Dynamic Systems, Measurement, and Control*, *107*(1), 93–96.

Peterbilt Motors Company. (2010). Peterbilt Green Technologies. Retrieved from http://www.peterbilt.com/eco/index.htm

Peterbilt Motors Company. (2011). Peterbilt Motors Company. Retrieved November 3, 2011, from http://www.peterbilt.com/index.aspx

Pourmovahed, A., Beachley, N. H., & Fronczak, F. J. (1992). Modeling of a Hydraulic Energy Regeneration System: Part I—Analytical Treatment. *Journal of Dynamic Systems, Measurement, and Control*, *114*, 155.

Ratti, C., Townsend, A., Bettencourt, L. M. A., West, G. B., McGranahan, G., Satterthwaite, D., Biello, D., et al. (2011). 38 Street-Savvy. *Scientific American*, *305*(3), 39-41.

Rush Enterprises. (2006). Rush Truck Centers - Search Results. Retrieved October 17, 2011, from http://www.rushtruckcenters.com/search_results.aspx?loc=&xloc=&type=New+Heavy+Duty&mkmdl=Peterbilt%7c320

SAE Truck and Bus Engine Preformance and Application Subcommittee. (2000). *Information Relating to Duty Cycles and Average Power Requirements of Truck and Bus Engine Accessories* (Standard No. SAE J1343). Warrendale, PA: SAE International.

Shan, M. (2009). *Modeling and control strategy for series hydraulic hybrid vehicles*. The University of Toledo.

Soderberg, P. (2011, March). Less is More. *International Industrial Vehicle Technology*, *19*(1), 92-93.

Sutton, R. S., & Barto, A. G. (1998). *Reinforcement Learning: An Introduction*. Cambridge, MA: The MIT Press.

Svoboda, J., Bouchard, G., & Katz, S. (1978). A Thermal Model for Gas-Charged Accumulators Based on the Heat Conduction Distribution. *Fluid Transients and Acoustics in the Power Industry*.

Texas Dept. of Transportation. (2011). Texas Legal Size and Weight Limits. Retrieved from http://www.dot.state.tx.us/business/motor_carrier/overweight_permit/weight_limits.htm

Texas State Data Center. (2009, June 3). Texas Population Projections Program. Retrieved June 4, 2011, from http://txsdc.utsa.edu/tpepp/2008projections/

U.S. Census Bureau. (2009). Population Projections - 2009 National Population Projections. Retrieved June 4, 2011, from http://www.census.gov/population/www/projections/2009projections.html

U.S. Department of Energy. (2011). Weekly Retail On-Highway Diesel Prices. Retrieved from http://tonto.eia.doe.gov/oog/info/wohdp/diesel.asp

U.S. Environmental Protection Agency Office of Air and Radiation. (2011, April). The Benefits and Costs of the Clean Air Act from 1990 to 2020. Retrieved from http://www.epa.gov/air/sect812/feb11/fullreport.pdf

United States Environmental Protection Agency. (2010). Clean Automotive Technology: Hydraulic Hybrid Research. Retrieved from http://www.epa.gov/otaq/technology/research/research-hhvs.htm

United States Environmental Protection Agency. (2011, August). EPA and NHTSA Adopt First-Ever Program to Reduce Greenhouse Gas Emissions and Improve Fuel Efficiency of Medium-and Heavy-Duty Vehicles. Retrieved from http://www.epa.gov/otaq/climate/documents/420f11031.pdf

Wong, J. Y. (2008). *Theory of Ground Vehicles* (4th ed.). Hoboken, New Jersey: John Wiley & Sons, Inc.

Wu, Bin, Lin, C. C., Filipi, Z., Peng, H., & Assanis, D. (2004). Optimal Power Management for a Hydraulic Hybrid Delivery Truck. *Vehicle System Dynamics*, *42*(1-2), 23-40.